*buildings*

MDPI

*Article*

# A Comparison Analysis of Buildings as per Norwegian and Ethiopia ES-EN1998-1 Seismic Code

**Mistreselasie Abate [1], Ana Catarina Jorge Evangelista [1,*] and Vivian W. Y. Tam [2]**

[1] School of Engineering, Civil Engineering, Engineering Institute of Technology, Perth, WA 6005, Australia; 12536@student.eit.edu.au
[2] School of Engineering, Design and Built Environment, Western Sydney University, Penrith, NSW 2751, Australia; v.tam@westernsydney.edu.au
* Correspondence: ana.evangelista@eit.edu.au

**Abstract:** An earthquake is one of the most significant and shocking natural disasters ever documented anywhere on the planet. Throughout history, it has claimed millions of lives and wreaked devastation on infrastructure. Because earthquake forces are spontaneous and unpredictable, engineering methods must be honed to investigate buildings under the impact of these forces. The dynamic and static computations of four RC multistory structure prototypes with various elevations in a high seismic zone are compared in this paper. The project under review is modeled as a 3, 6, 12, and 18-story establishment, and it is analyzed employing ETABS vs. 2019. The Equivalent Lateral Force (ELF) Procedure is used for static experimentation, while the Response Spectrum (RS) Procedure is employed for dynamic investigation. Both calculations are performed as per the EUROCODE 8-2004 recommendation. The ELF seismic load practice utilized was for the country of Norway, which has similar parameters to the ES-EN 8-15 seismic regulation Type I target RS, with ag/g = 0.1, spectrum type = I, soil factor S = 1.3 ground type, spectrum period (Tb, Tc, and Td) 0.1 s, 0.25 s, and 1.5 s. For the RS investigation, the parameters employed are as per ESEN-2015, ag/g = 0.1, and the spectrum type = I and ground type = B parameters were involved in the same manner for the RS analysis. The soil factor was set to 1.35; the spectrum period was set to (Tb, Tc, and Td) 0.05 s, 0.25 s, and 1.2 s. The behavior factor = 3.8, the lower bound factor = 0.2, and the damping ratio = 0.05. The results are then compared by employing different components such as displacement, story drift, story stiffness, base story shear, and story moment. Ultimately, a comparison of static and dynamic investigations has been carried out. Compared to the RS approach, the ELF technique produces more additional displacement, total drift, and base shear. As per the findings of this paper, for high-rise and tall buildings, dynamic analysis such as RS should be used rather than static analysis (ELF).

**Keywords:** base shear; equivalent lateral force; story drift; response spectrum; displacement; static analysis; dynamic analysis; linear analysis



**Citation:** Abate, M.; Evangelista, A.C.J.; Tam, V.W.Y. A Comparison Analysis of Buildings as per Norwegian and Ethiopia ES-EN1998-1 Seismic Code. *Buildings* **2024**, *14*, 1841. https://doi.org/10.3390/buildings14061841

Academic Editors: Humberto Varum, Cong Ma, Haijun Zhou, Rujin Ma and Rui Zhou

Received: 13 March 2024
Revised: 9 May 2024
Accepted: 12 June 2024
Published: 17 June 2024



## 1. Introduction

Due to the world's growing population, creating low- to high-rise structures that can withstand lateral dynamic stresses induced by earthquakes is becoming more fashionable. The impacts of earthquakes are more potent than the effects of wind. Many buildings have been destroyed as a result of natural and unexpected earthquakes that induce tremendous ground shaking, as shown by previous severe disasters. As a result, tremor analysis and design are critical in today's society. The ELF and RS techniques used in this investigation were performed following EUROCODE 8-2004 and the Norwegian building code.

## 2. Literature Review

This research includes an investigation of the seismic behavior of high-rise structures, such as the Fortune One Tower, which is approximately twenty-two stories with four basements and is found in Jinnah Avenue (Sector F-9), Islamabad. (Zone-2B) [1–3]. The project

aims to specify the most cost-effective structural component sizes while providing the suggested structure's safety, stability, and serviceability. ETABS 2016 was utilized to model the structure [4–7]. The chosen design was subjected to linear static and linear dynamic investigations. A static study used the ELF approach, whereas a dynamic investigation was conducted using RSA. The structure was designed utilizing the Pakistan Building Code (BCP), the UBC-97, and the ACI 318-14 conditions [8–10]. The cost-effective sizes of structural components are the result of this study. The response spectrum analysis procedure was authenticated to be better than the equivalent lateral force method [11–18].

The location of an earthquake at a multi-story building clearly illustrates that buildings built poorly and without abundant strength will fall apart when the earthquake happens [19–23]. To ensure the safety of multi-story structures against seismic forces, the seismic investigation must be studied, and earthquake-resistant systems must be developed [24]. In structural seismic investigation, the response spectrum analysis approach is applied. The seismic investigation used was a residential building with G+13 stories in zone III [24]—the STAAD. The Pro V8i program analyzes the complete structure [24]. This work investigates the effect of a significant number of vertically displaced, geometrically imperfect components on the seismic response of a structure [25]. For this project, the primary purpose is to use the RSA on RC buildings with inconsistent vertical frames and design methods/standards based on IS 13920 to perform RSA design using the ductility procedure [26]. The findings from analyzing the irregular structure are contrasted with those from the study of the regular structure [24]. "The researchers examined three forms of irregularities: mass irregularity, stiffness irregularity, and stiffness and mass irregularity" [27]. According to the observations, the maximum story shear force was found to be highest in the first story and lowest in the top story in all illustrations [28]. The base shear in mass irregular structures was shown to be more significant than in identical regular structures [24]. The stiff, uneven structure had higher inter-story drifts and survived less base shear [24].

The New Zealand Building Code's current dynamic moment and shear force magnification requirements in cantilever wall constructions are scrutinized [29]. Higher mode effects are insufficiently captured by either the relative ELF or modal RS design procedures, according to time–history assessments of six wall constructions ranging in height from two to twenty stories [30]. According to the time–history data, dynamic amplification depends on both starting periods and predicted displacement ductility levels. Using two alternative methodologies, higher mode properties in cantilever walls are considered [31]. The first is based on a straightforward adaptation of the modal RS method, while the second is appropriate for single-mode design methods like the ELF method. Both provide a good characterization of the predicted reaction [32]. It is revealed that providing capacity protection at the design seismic intensity does not promise that undesired catastrophe modes will not happen at intensities larger than the design level. This has consequences for the design of crucial infrastructure, such as hospitals [33].

In another study, the building was planned according to code requirements, which imposed several limits while analyzing dynamic loads [34]. This time-consuming and complicated analytical technique takes a long time to complete. As a result, most structures are constructed on the premise of static loading [35]. In the event of a disaster, such as an earthquake, overlooking the dynamic forces may collapse the whole building. Recent earthquakes have shown the importance of dynamic analysis [36]. Most research is now being accomplished on dynamic analysis to ensure that structures can sustain earthquake-induced strains. Several theoretical formulae exist in various nations' seismic regulations that relate the building's height to the building's omega, or natural period of vibration [37,38]. The lateral forces are predicted using the acceleration spectrum in this technique. The displacement demand provides a detailed estimate of the damage to be expected [39]. The essential periods of a case study of a low-rise structure are examined in this research utilizing the ELF and RS, all of which are based on IS 1893 (Part 1), as well as FEM in seism structure [40]. These techniques' basic periods correspond to 0.39 s,

0.14 s, and 0.178 s. The components determining a structure's fundamental period are explained [41]. The findings, however, demonstrate an appropriate error in the range (1–30%), and the seism struct provided genuine natural frequency calculations since the Indian code has a regular mode shape. This work also examines the limits of doing modal analysis [42].

All structures are directly affected by earthquakes. The consequences vary depending on the zone where earthquakes occur. The state and varieties of medium, hard, and soft soil impact how buildings react to earthquake loads. Because the soil grades of these soils' conditions are so variable, seismic waves flow through the strata in different ways [43,44]. During earthquakes, the foundations of structures interact with the soil underneath. In conclusion, the type of soil and building directly disturb the ground structure and the consequences of the earthquake it experiences [45]. As a result, several evaluations of the same building in diverse seismic zones are carried out by changing the soil type for each simulation among hard, medium, and soft. Responses such as tale drift and displacement are shown for various zones and soil types [46]. The RS requirements for simulations in these different soil types are provided in IS 1893:2016, "Criteria for Earthquake Resistant Design of Structures". This study has significant implications for structural design and geotechnical engineering [47].

As the world's population continues to rise, there is an excellent demand for high-rise construction [48]. All across the globe, these establishments are utilized for residential, commercial, and industrial motivations [49]. Because natural catastrophes such as earthquakes are unexpected, the seismic resilience of these buildings is critical [50]. Bracings are essential to neutralize lateral loads, which may boost a building's earthquake resistance capability [49]. "Using STAAD Pro V8i and the response spectrum and analogous static methods, this paper investigated the seismic manners of a G+41 story steel frame with concrete slab under X, K, and V bracings" [49]. All of the frames were tested for story displacement and base shear. V bracing, out of all the analyzed bracings, provided the structure with the most effective seismic protection [50].

In urban India, reinforced concrete frame structures are the most common building [51]. A structure is subjected to various static and dynamic forces during its existence [52]. The self-weight of the building is the primary source of static forces, which are time-independent. Dynamic forces, which include earthquake forces, are, on the other hand, time-dependent [53]. Both static and dynamic procedures may be used to conduct seismic analysis on RC structures. "The static technique assumes that the rate at which the load is applied is too sluggish to create substantial inertia forces in the structure, whereas the dynamic method considers inertia forces" [54]. Static approaches can only serve the purpose for low- to medium-rise structures, while dynamic analysis becomes critical for high-rise buildings, which are the most impacted by earthquake forces [55]. Buildings are increasingly becoming higher and thinner as demand grows and land availability shrinks [51]. As a result, dynamic analysis has generated vitality in a nation like India, which has been severely discouraged by strong earthquakes in the past, inflicting significant harm to infrastructure and human lives [51]. The ELF and the RS, both dynamic and static methods, are the most broadly used seismic analysis methods [56]. The equivalent static method is appropriate for typical structures under 15 m in height in seismic zone II. At the same time, the linear dynamic method is recommended for all other buildings, as per Indian standard regulations [57]. However, it has been noticed that the ELF method is also used in design practice for structures of more than 15 m in different seismic zones [54]. Using ETABS v. 2019 structural analysis software, this paper employs the ELF and RS methods to analyze multi-story framed structures of varying heights across different seismic zones. A comparative assessment is conducted between the outcomes of both methods, focusing on responses like bending moments, axial forces, and nodal displacements [57]. The most suitable and precise of the two ways of analyzing RC structure is selected based on the comparisons [58].

Using the force-based design technique (FBD) and the direct displacement-based design approach, this research investigates the seismic behavior of low-, medium-, and high-rise RC-framed building models (DDBD) [52]. Four-story, eight-story, and twelve-story RC-framed building models were used in the inquiry as low-, medium-, and high-rise structures, respectively [50]. The program ETABS was employed to model, analyze, and design the buildings [28]. For the building models, criteria such as base shear, story displacement, story drift, hinge formation, and reinforcing needs were explored and compared [48]. The analysis and design results revealed that the latter method is more cost-effective than the FBD method [28]. The DDBD is more conformed for medium-rise structures than low-, medium-, and high-rise buildings under consideration [28].

According to another investigation in the early days of civil engineering, buildings were continually constructed with the static load factor in mind. Subsequently, advancements in civil engineering studies showed that structures are subject to a collection of additional loads, enclosing seismic forces, wind pressures, snow loads, and various others, contingent upon factors such as the structure's sizes, geographical placement, soil conditions, and other pertinent variables. "As a result, the procedure of assessing a design for many types of loads and designing the system for the essential load requirement was presented, with the dynamic load standing as one of the major loads for which the system should be evaluated and developed". The preliminary objective of this investigation is to examine the seismic persistence of a multistory RC moment-resistant articulated structure under static and dynamic hurdles by BNBC, 2006 [10,43]. The structure was subjected to a static seismic load using the equivalent static force (ESF) technique. Nevertheless, the response spectrum (RS) approach implemented dynamic loading [41]. "The current investigation examines the divergences in story displacement and drift for each story, as well as base shear, story stiffness, bending moments, and story shear forces in columns at various story levels" [40]. Finally, a comparison of static and dynamic analysis has been carried out [20]. According to computational modeling output data, the base shear obtained by RS analysis is smaller than that obtained from the ESF procedure [39]. The maximum story displacement obtained from dynamic response spectrum analysis is approximately 78% of that obtained from static analysis [15,59]. Simultaneously, an internal column's dynamic maximum bending moment is approximately 87% of its static counterpart [60].

Furthermore, in another study [15], the most favored kinds of construction in urban India are reinforced concrete (RC) building frames. During their lifespan, they are exposed to various forces, including static forces from DL and LL as well as dynamic forces from earthquakes [15]. In this investigation, two towering construction methods, G+10 and +25, in seismic zone III are analyzed, employing two different strategies: ELF and RS, both of which are performed in ETABS 15 [15]. "For comparison investigation, factors such as story drift, story displacement, axial load, and bending moments are calculated from the analytical findings. The response spectrum approach was better than the equivalent static analysis method" [15].

For structural design and evaluation, numerous seismic analysis methodologies have been defined in the most current standards. Because various techniques have varied benefits and disadvantages, a thorough comparison is necessary to determine which is most successful [30]. The numerous ordinary methods are the ELF procedure, the modal response MRS, and the LRH investigation [29]. This research intends to provide a comparative analysis of various approaches using ETABS v. 2019 software by the ASCE 7-16 standard. Six different types of buildings designed as per ACI 318-19 norms were investigated in terms of base shear and the allocation of story shear forces [58]. In areas prone to high seismic activity, building code specifications for reinforced concrete buildings equipped with a dual lateral force-resisting system undergo scrutiny [61]. Compared to the MRS or LRH analyses, the ELF procedure's base shear for the building under investigation is conservative [61]. The ELF procedure's vertical distribution is simply a function of the structure's basic period; however, the MRS and LRH analyses have the advantage

of exposing how a structure's mass and stiffness distribution affects member forces and displacements [61–63].

### *2.1. Gap in the Literature*

Following an extensive literature review, research was conducted globally on equivalent lateral force (ELF) and response spectrum (RS) analyses. However, to our knowledge, there is a lack of comparable studies on ELF and RS calculations for 3-, 6-, 12-, and 18-story moment-resisting frame systems in the chosen design region of Ethiopia. This comparative analysis holds significance due to adherence to the Type I response spectrum outlined in the Ethiopian Building Code ES EN 1989-1:2015 and the Norwegian Building Code. Various parameters, encompassing both local and global structural responses, are included in the comparison.

### *2.2. The Objective of the Research*

This study compares structures under earthquake motions, employing static (ELF) and dynamic (RS) analyses. The analysis focuses on reinforced concrete framed structures with varying story heights in a high seismicity zone, adhering to EUROCODE 8-2004 standards. The ELF seismic load pattern utilized corresponds to that of Norway, which shares parameters similar to those of the Building Code of Ethiopia ESEN-2015, as depicted in Figures A1 and A2, Tables A1 and A2. To achieve this, four models with different heights were created and analyzed using ETABS 2019, with results compared across five parameters: story moment, displacement, story shear, story drift, and base shear.

## 3. Case Study—Description

This study focuses on a standard reinforced concrete building, depicted in Table 1, Figures 1, 2 and 3a–d. The floor area of the structure spans 900 square meters, measuring 30 m by 30 m, and includes five bays along each side, with individual spans measuring 6 m. The structure is modeled in three variations: 3, 6, 12, and 18 stories, each with a height of 3.20 m.

**Table 1.** Sample RC buildings detail.

| Property for 3-, 6-, 12-, and 18-Story RC Sample Building | Description |
|---|---|
| Height for 3-, 6-, 12-, and 18-story RC | 9, 18, 36, 54 m |
| Structure's type | Multi-story moment-resisting frame (3, 6, 12, and 18 story) |
| Floor-to-floor height | 3 m |
| Soil type | B |
| Damping | 0.05 |
| Support | Fixed support |
| Importance factor | 1 |
| R factor | 3.8 |
| Beam section | 500 × 350 mm |
| Column section | 400 × 400 mm |
| Wall section | 300 mm |
| Slab section | 200 mm |
| Seismic zone | 3 (Addis Ababa) |
| Concrete quality | C-30 |
| Steel | G-60 |

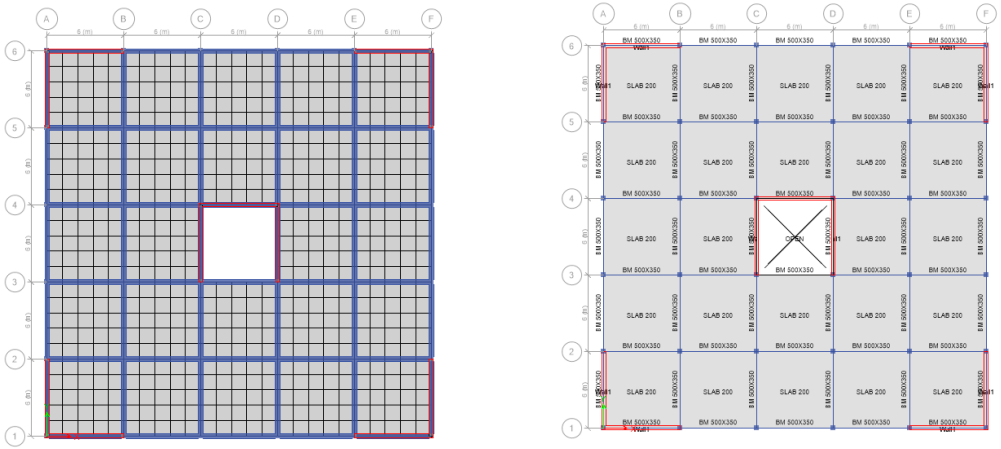

(**a**) (**b**)

**Figure 1.** (**a**) Plan view of sample meshed RC structure. (**b**) Plan view of sample RC structure with section detail.

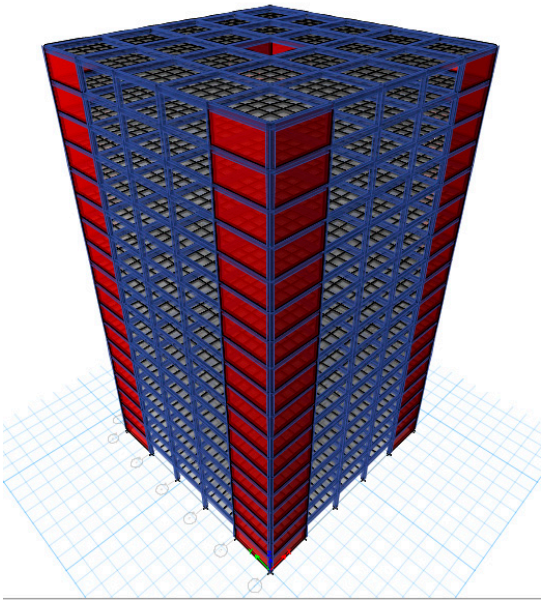

**Figure 2.** Sample ETABS model.

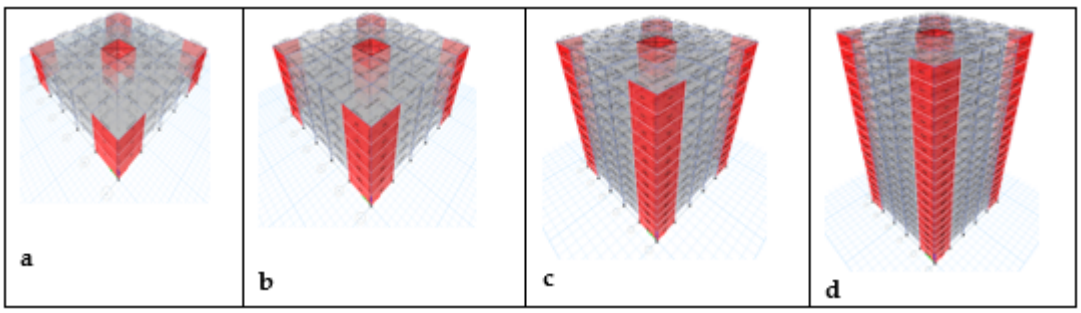


**Figure 3.** (**a**) Sample 3-story building; (**b**) sample 6-story building; (**c**) sample 12=story building; and (**d**) Sample 18-story building.

Different loads operating on a building play an essential role in its design. The failure of a structure may be caused by a mistake in estimating these loads. As a result, a thorough examination of the loads operating on the structure is required. The loads in a particular region must be carefully chosen, and the worst possible combination of these loads must be assessed. The weight of all walls, partitions, floors, and roofs, as well as the weight of any other permanent structures in the building, should be included in the dead load. The dead load (DL) is computed as 2 kN/m$^2$ based on the materials used in the construction. The live load (LL) is measured at 3 kN/m$^2$. The construction is said to be in a seismically active location near Addis Ababa, Ethiopia. Table 2 shows the seismic parameters employed in this research, which are based on ES8-15, corresponding to Eurocode 8-2004 standards (based on EN1998-1) and the Norwegian Building Code.

**Table 2.** Loading Detail.

| | |
|---|---|
| Dead load | 2 kN/m$^2$ |
| Live load | 3 kN/m$^2$ |
| Wall load on beam | 12 kN/m$^2$ |
| ELF and RS procedure | ES8-15 corresponds to Eurocode 8-2004 standards (based on EN1998-1) and Norwegian Building Code |

## 4. Modeling and Analysis

Various configurations with different dimensions were simulated and assessed using ETABS 2019, employing ELF for static analysis and RS for dynamic investigation following ES8-15 and the Norwegian Building Code, adhering to Eurocode 8-2004 standards. The modeling of different systems in the software v. 19 is depicted in Figure 2.

## 5. Results and Discussion

Ultimately, the internal forces calculated from the static and dynamic analysis of the structures at different heights were compared for all five criteria: displacement, story drift, base shear, story shear, and story moment.

### *5.1. Three-Story Building*

Table 3, Figures A3a, A7a, A9b and 4 illustrate the three-story CM displacement for diaphragm D1 by dynamically and statically analyzing the sample structure results. It can be seen that the maximum SMD obtained by RS is higher than that obtained by ELF for all the stories. The ELF result indicated 73.188% in the X-axis and 73.44% in the Y-axis of the RS results. It can be observed that the difference in CMD generated by both methods decreased from the bottom to the top of the structure in both X and Y directions.

**Table 3.** CM displacement for diaphragm D1 for three-story structure by static and dynamic analysis.

| | | **ELF X-Y Axis Output** | | **RS X-Y Axis Output** | | **X-Y Axis Output** | |
|---|---|---|---|---|---|---|---|
| | | **CM Displacement for Diaphragm D1** | | **CM Displacement for Diaphragm D1** | | **CM Displacement for Diaphragm D1** | |
| **Elevation** | **Location** | **X-Dir** | **Y-Dir** | **X-Dir** | **Y-Dir** | **ELF vs. RS X-Dir** | **ELF vs. RS Y-Dir** |
| m | | mm | mm | mm | mm | % | % |
| 9 | Top | 1.313 | 1.189 | 1.794 | 1.619 | 73.188 | 73.440 |
| 6 | Top | 0.871 | 0.774 | 1.186 | 1.05 | 73.440 | 73.714 |
| 3 | Top | 0.38 | 0.331 | 0.516 | 0.446 | 73.643 | 74.215 |
| 0 | Top | 0 | 0 | 0 | 0 | 0 | 0 |

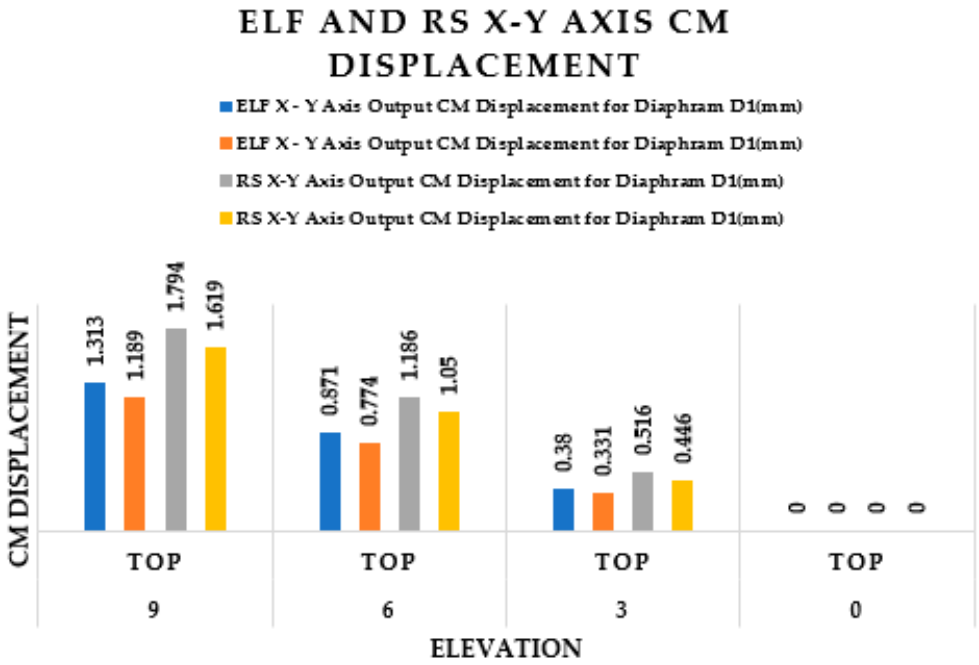


**Figure 4.** ELF and RS X-Y axis CM displacement.

Table 4, Figures A3b, A7b, A10a and 5 illustrate the three-story drift for diaphragm D1 by dynamically and statically analyzing the sample structure results. It can be seen that the maximum DFD obtained by RS is higher than that obtained by ELF for all the stories. The ELF result indicated 71.97% in X—the X-axis and 73.82% in the Y-axis of the RS results. It has been observed that the difference in DFD generated by both methods decreases from the bottom to the top of the structure in both X and Y directions.

**Table 4.** Comparison of static and dynamic analysis results for CM drifts for diaphragm D1 for three-story structures.

| | | **ELF X-Y Axis Output** | | **RS X-Y Axis Output** | | **X-Y Axis Output** | |
|---|---|---|---|---|---|---|---|
| | | **Drifts for Diaphragm D1** | | **Drifts for Diaphragm D1** | | **Drifts for Diaphragm D1** | |
| **Elevation** | **Location** | **X-Dir** | **Y-Dir** | **X-Dir** | **Y-Dir** | **ELF vs. RS X-Dir** | **ELF vs. RS Y-Dir** |
| m | | | | | | % | % |
| 9 | Top | 0.000154 | 0.000138 | 0.000218 | 0.000191 | 70.642 | 72.251 |
| 6 | Top | 0.00017 | 0.000148 | 0.000238 | 0.000202 | 71.428 | 73.267 |
| 3 | Top | 0.000131 | 0.00011 | 0.000182 | 0.000149 | 71.978 | 73.825 |
| 0 | Top | 0 | 0 | 0 | 0 | 0 | 0 |

Table 5, Figures A4a, A8a, A11a and 6 illustrate the three-story max story displacement by dynamically and statically analyzing the sample structure results. It can be seen that the maximum MSD obtained by RS is higher than that obtained by ELF for all the stories. The ELF result indicated 71.92% in the X-axis and 74.04% in the Y-axis of the RS results. It can be observed that the difference in MSD generated by both methods decreases from the bottom to the top of the structure in both X and Y directions.

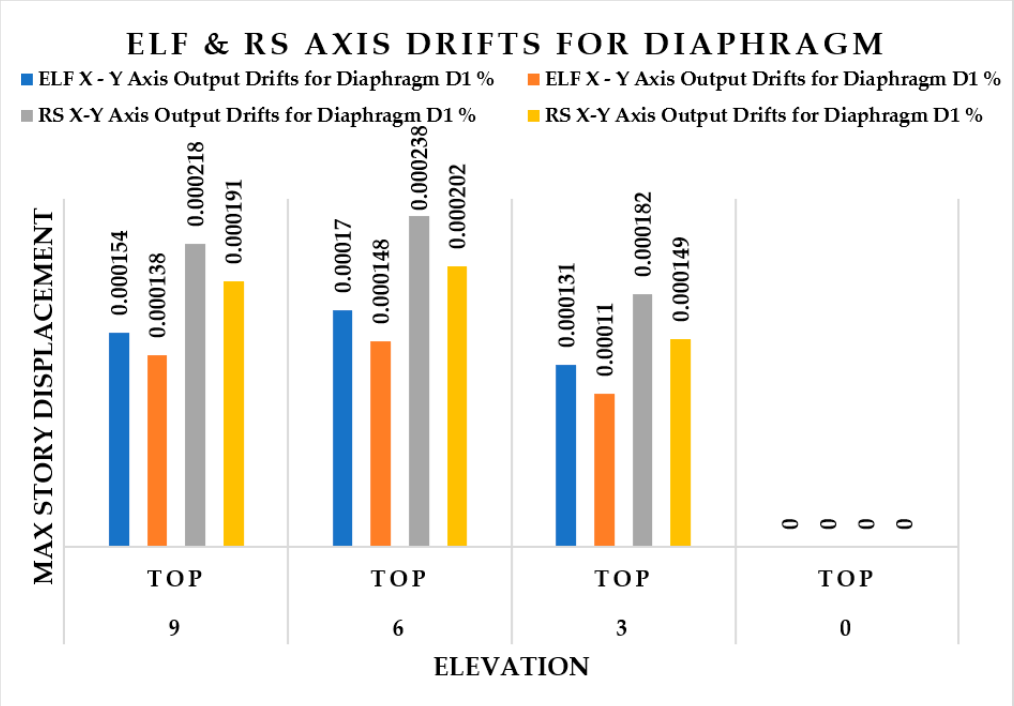


**Figure 5.** ELF and RS X-Y axis drifts for diaphragm.

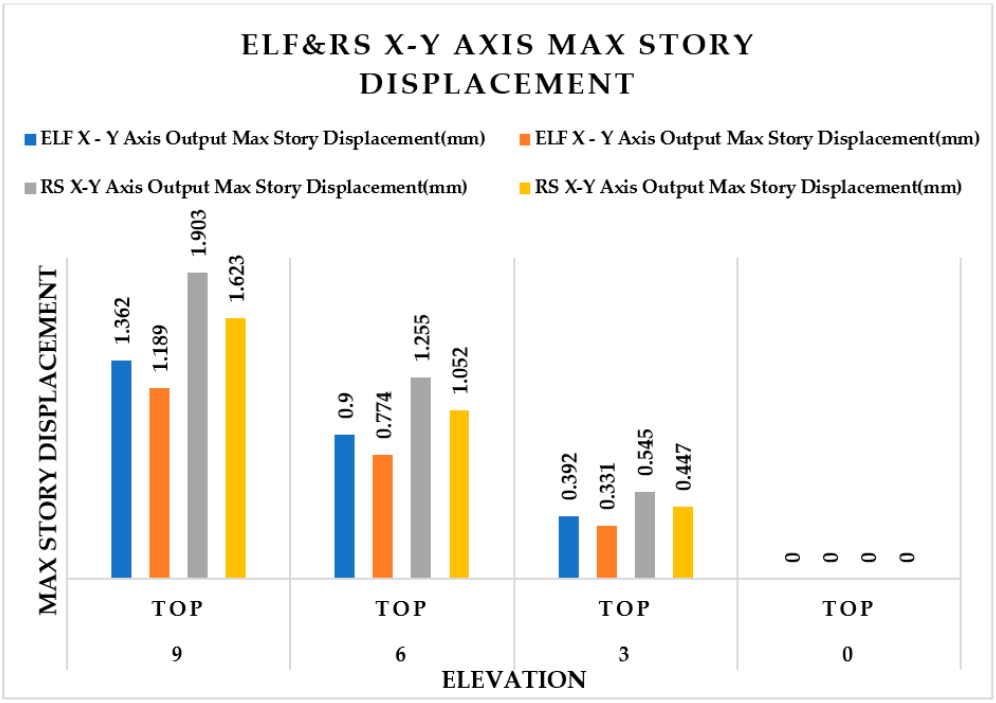


**Figure 6.** ELF and RS X-Y axis max story displacement.

**Table 5.** Comparison of static and dynamic analysis results in max story displacement for three-story structures.

| | | ELF X-Y Axis Output | | RS X-Y Axis Output | | X-Y Axis Output | |
|---|---|---|---|---|---|---|---|
| | | Max Story Displacement | | Max Story Displacement | | Max Story Displacement | |
| Elevation | Location | X-Dir | Y-Dir | X-Dir | Y-Dir | ELF vs. RS X-Dir | ELF vs. RS Y-Dir |
| m | | mm | mm | mm | mm | % | % |
| 9 | Top | 1.362 | 1.189 | 1.903 | 1.623 | 71.571 | 73.259 |
| 6 | Top | 0.9 | 0.774 | 1.255 | 1.052 | 71.713 | 73.574 |
| 3 | Top | 0.392 | 0.331 | 0.545 | 0.447 | 71.926 | 74.049 |
| 0 | Top | 0 | 0 | 0 | 0 | 0 | 0 |

Table 6, Figures A4b, A10b and 7 illustrate the three-story max story drifts by dynamically and statically analyzing the sample structure results. It can be seen that the maximum MSD obtained by RS is higher than that obtained by ELF for all the stories. The ELF result indicated 71.97% in the X-axis and 73.82% in the Y-axis of the RS results. It can be observed that the difference in MSD generated by both methods decreases from the bottom to the top of the structure in both X and Y directions.

**Table 6.** Comparison of static and dynamic analysis results for max story drifts for three-story structures.

| | | ELF X-Y Axis Output | | RS X-Y Axis Output | | X-Y Axis Output | |
|---|---|---|---|---|---|---|---|
| | | Max. Story Drifts | | Max. Story Drifts | | Max. Story Drifts | |
| Elevation | Location | X-Dir | Y-Dir | X-Dir | Y-Dir | ELF vs. RS X-Dir | ELF vs. RS Y-Dir |
| m | | | | | | % | % |
| 9 | Top | 0.000154 | 0.000138 | 0.000218 | 0.000191 | 70.642 | 72.251 |
| 6 | Top | 0.00017 | 0.000148 | 0.000238 | 0.000202 | 71.428 | 73.267 |
| 3 | Top | 0.000131 | 0.00011 | 0.000182 | 0.000149 | 71.978 | 73.825 |
| 0 | Top | 0 | 0 | 0 | 0 | 0 | 0 |

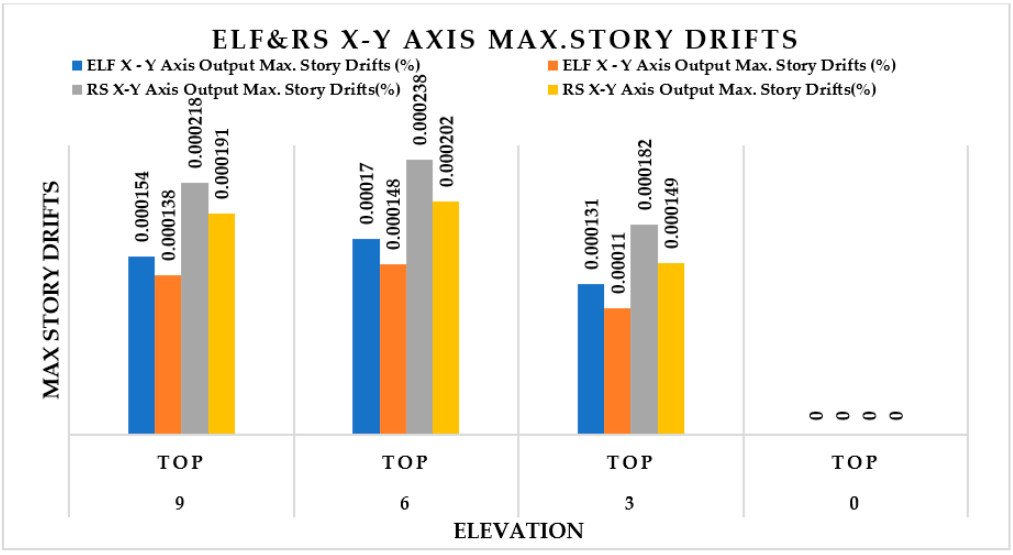


**Figure 7.** ELF and RS X-Y axis max story drifts.

Table 7, Figures A5a, A8b, A12b and 8 illustrate the three-story max story shear by dynamically and statically analyzing the sample structure results. It can be seen that the

maximum MSD obtained by RS is higher than that obtained by ELF for all the stories. The ELF results indicated 73.68% on the X-axis and 74.20% on the Y-axis of the RS results. It can be observed that the difference in MSD generated by both methods decreases from the bottom to the top of the structure in both X and Y directions.

**Table 7.** Comparison of static and dynamic analysis results in story shears for three-story structures.

| | ELF X-Y Axis Output | | | RS X-Y Axis Output | | X-Y Axis Output | |
|---|---|---|---|---|---|---|---|
| | | Story Shears | | Story Shears | | Story Shears | |
| Elevation | Location | X-Dir | Y-Dir | X-Dir | Y-Dir | ELF vs. RS X-Dir | ELF vs. RS Y-Dir |
| m | | kN | kN | kN | kN | % kN | % kN |
| 9 | Top | −4684.32 | −4684.3181 | 6634.351 | 6656.891 | −70.607 | −70.367 |
| | Bottom | −4684.32 | −4684.3181 | 6634.351 | 6656.891 | −70.607 | −70.367 |
| 6 | Top | −8049.99 | −8049.9904 | 11053.03 | 11028.78 | −72.830 | −72.990 |
| | Bottom | −8049.99 | −8049.9904 | 11053.03 | 11028.78 | −72.830 | −72.990 |
| 3 | Top | −9732.83 | −9732.8265 | 13209.4 | 13116.83 | −73.681 | −74.201 |
| | Bottom | −9732.83 | −9732.8265 | 13209.4 | 13116.83 | −73.681 | −74.201 |
| 0 | Top | 0 | 0 | 0 | 0 | 0 | 0 |

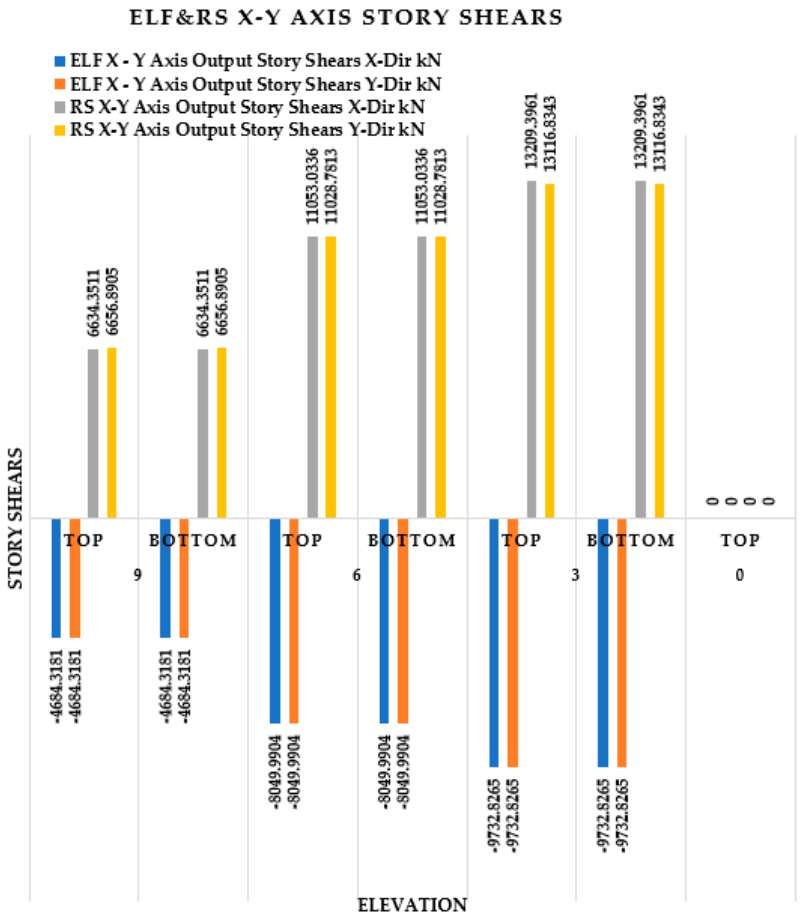


**Figure 8.** ELF and RS X-Y axis max story shear.

Table 8, Figure A6a,b, Figures A11b and 9 illustrate the three-story max overturning moment by dynamically and statically analyzing the sample structure results. It can be seen that the maximum MOM obtained by RS is higher than that obtained by ELF for all the stories. The ELF result indicated 73.75% on the X-axis and 73.56% on the Y-axis of the

RS results. It can be observed that the difference in MOM generated by both methods decreases from the bottom to the top of the structure in both X and Y directions.

**Table 8.** Comparison of static and dynamic analysis results for overturning moment for three-story structures.

| | | ELF X-Y Axis Output | | RS X-Y Axis Output | | X-Y Axis Output | |
|---|---|---|---|---|---|---|---|
| | | Overturning Moment | | Overturning Moment | | Overturning Moment | |
| Elevation | Location | X-Dir | Y-Dir | X-Dir | Y-Dir | ELF vs. RS X-Dir | ELF vs. RS Y-Dir |
| m | | kN-m | kN-m | kN-m | kN-m | % kN-m | % kN-m |
| 9 | Top | 0 | 0 | 0 | 0 | 0 | 0 |
| 6 | Top | 14052.95 | −14052.9544 | 19970.67 | 19903.05 | 70.367 | −70.607 |
| 3 | Top | 38202.93 | −38202.9256 | 52741.39 | 52730.14 | 72.434 | −72.449 |
| 0 | Top | 67401.41 | −67401.4051 | 91389.9 | 91625.96 | 73.751 | −73.561 |

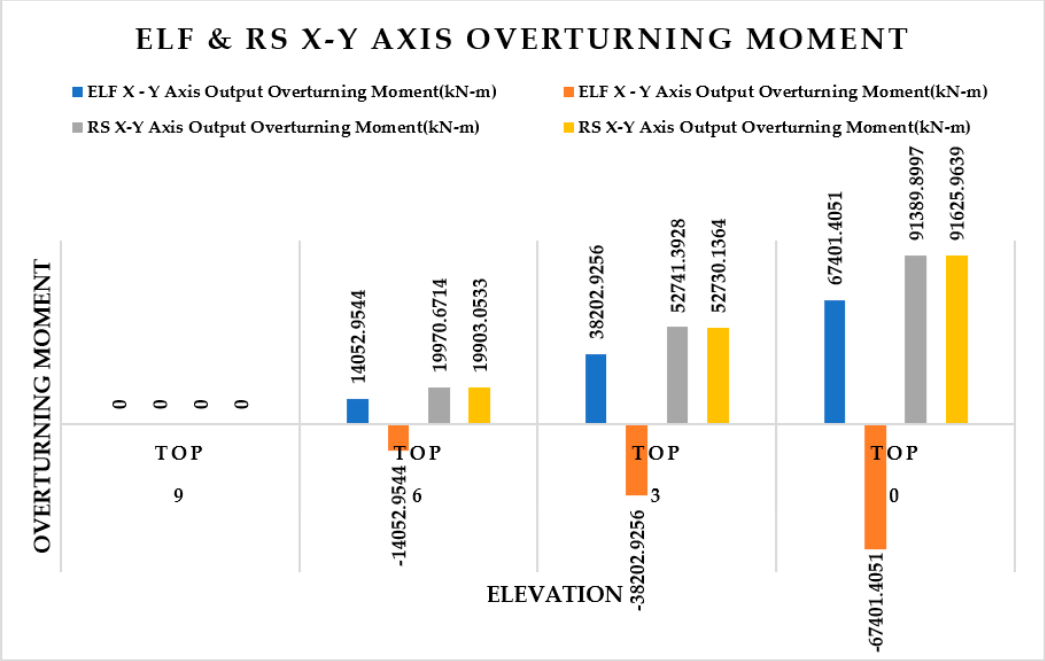


**Figure 9.** ELF and RS X-Y axis overturning moment.

*5.2. Six Story Building*

Table 9, Figures A13a, A16b, A20a and 10 illustrate the six-story CM displacement for diaphragm D1 by dynamically and statically analyzing the sample structure results. It can be seen that the maximum SMD obtained by RS is higher than that obtained by ELF for all the stories. The ELF result indicated 60.19% in the X-axis and 60.35% in the Y-axis of the RS results. It can be observed that the difference in CMD generated by both methods decreases from the bottom to the top of the structure in both X and Y directions.

Table 10, Figures A13b, A17a, A20b and 11 illustrate the six-story drift for diaphragm D1 by dynamically and statically analyzing the sample structure results. It can be seen that the maximum DFD obtained by RS is higher than ELF for the whole story. The ELF result indicated 59.38% in the X-axis and 60% in the Y-axis of the RS results. It can be observed that the difference in DFD generated by both methods decreases from the bottom to the top of the structure in both X and Y directions.

**Table 9.** Comparison of static and dynamic analysis results for CM displacement for diaphragm D1 for six-story structures.

| | | | ELF X-Y Axis Output | | RS X-Y Axis Output | | X-Y Axis Output | |
|---|---|---|---|---|---|---|---|---|
| | | | CM Displacement for Diaphragm D1 | | CM Displacement for Diaphragm D1 | | CM Displacement for Diaphragm D1 | |
| Story | Elevation | Location | X-Dir | Y-Dir | X-Dir | Y-Dir | ELF vs. RS X-Dir | ELF vs. RS Y-Dir |
| | m | | mm | mm | mm | mm | % | % |
| Story6 | 18 | Top | 6.129 | 6.13 | 10.32 | 10.349 | 59.389 | 59.232 |
| Story5 | 15 | Top | 5.003 | 4.944 | 8.394 | 8.316 | 59.602 | 59.451 |
| Story4 | 12 | Top | 3.806 | 3.709 | 6.358 | 6.21 | 59.861 | 59.726 |
| Story3 | 9 | Top | 2.599 | 2.492 | 4.325 | 4.151 | 60.092 | 60.033 |
| Story2 | 6 | Top | 1.477 | 1.385 | 2.452 | 2.299 | 60.236 | 60.243 |
| Story1 | 3 | Top | 0.555 | 0.504 | 0.922 | 0.835 | 60.195 | 60.359 |
| Base | 0 | Top | 0 | 0 | 0 | 0 | 0 | 0 |

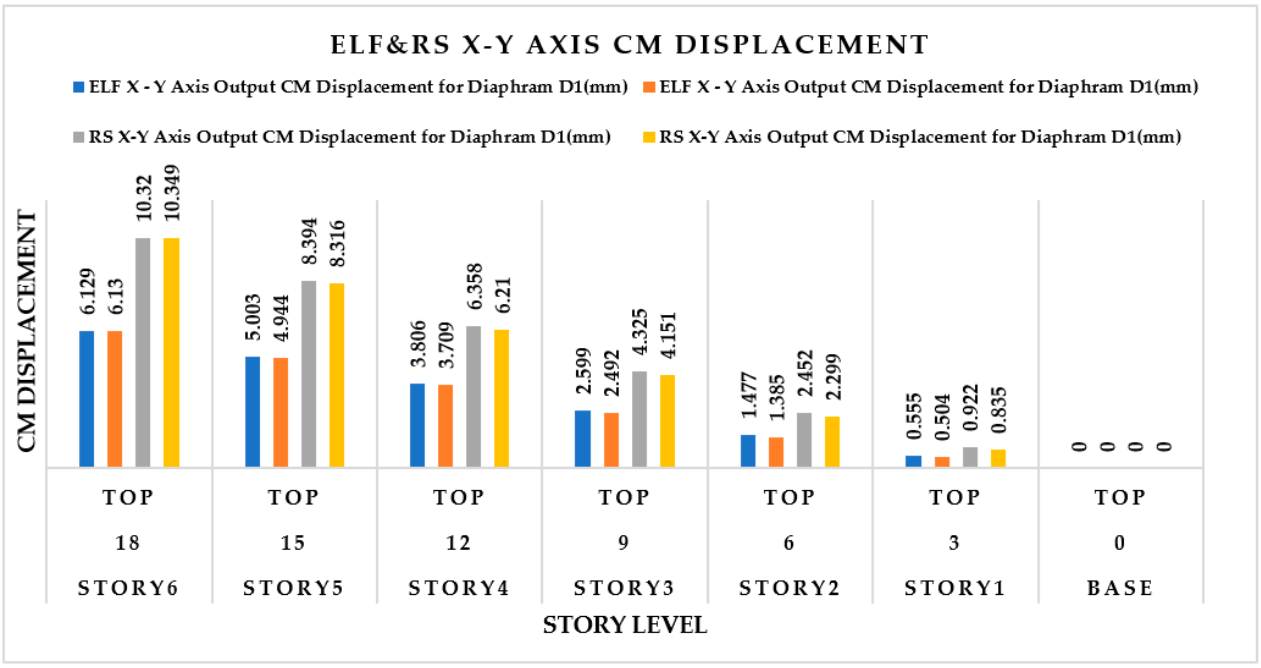


**Figure 10.** ELF and RS X-Y axis CM displacement.

**Table 10.** A comparison of static and dynamic analysis results in drifts for diaphragm D1 for six-story structures.

| | | | ELF X-Y Axis Output | | RS X-Y Axis Output | | X-Y Axis Output | |
|---|---|---|---|---|---|---|---|---|
| | | | Drifts for Diaphragm D1 | | Drifts for Diaphragm D1 | | Drifts for Diaphragm D1 | |
| Story | Elevation | Location | X-Dir | Y-Dir | X-Dir | Y-Dir | ELF vs. RS X-Dir | ELF vs. RS Y-Dir |
| | m | | | | | | % | % |
| Story6 | 18 | Top | 0.000397 | 0.000395 | 0.000705 | 0.000685 | 56.312 | 57.664 |
| Story5 | 15 | Top | 0.000421 | 0.000412 | 0.000745 | 0.000711 | 56.510 | 57.946 |
| Story4 | 12 | Top | 0.000423 | 0.000406 | 0.000741 | 0.000694 | 57.085 | 58.501 |
| Story3 | 9 | Top | 0.000392 | 0.000369 | 0.000679 | 0.000623 | 57.731 | 59.229 |
| Story2 | 6 | Top | 0.000321 | 0.000294 | 0.000551 | 0.000491 | 58.257 | 59.877 |
| Story1 | 3 | Top | 0.000192 | 0.000168 | 0.000329 | 0.00028 | 58.358 | 60 |
| Base | 0 | Top | 0 | 0 | 0 | 0 | 0 | 0 |

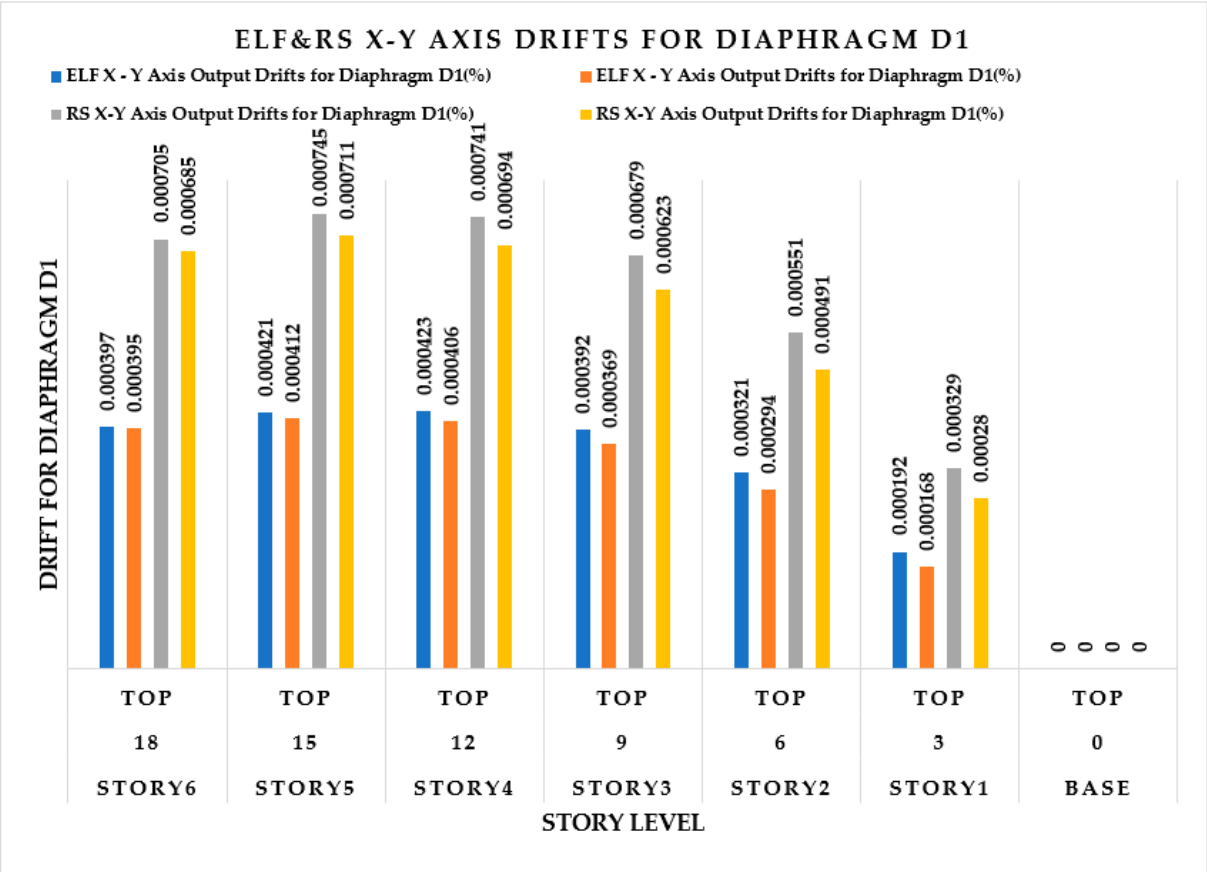


**Figure 11.** ELF and RS X-Y axis drifts for diaphragm D1.

Table 11, Figures A14, A17b, A21a and 12 illustrate the six-story max story displacement by dynamically and statically analyzing sample structure results. It can be seen that the maximum MSD obtained by RS is higher than that obtained by ELF for all the stories. The ELF result indicated 58.31% in the X-axis and 60% in the Y-axis of the RS results. It can be observed that the difference in MSD generated by both methods decreases from the bottom to the top of the structure in both X and Y directions.

**Table 11.** Comparison of static and dynamic analysis results in max story displacement for six-story structures.

| | | | **ELF X-Y Axis Output** | | **RS X-Y Axis Output** | | **X-Y Axis Output** | |
|---|---|---|---|---|---|---|---|---|
| | | | **Max Story Displacement** | | **Max Story Displacement** | | **Max Story Displacement** | |
| **Story** | **Elevation** | **Location** | **X-Dir** | **Y-Dir** | **X-Dir** | **Y-Dir** | **ELF vs. RS X-Dir** | **ELF vs. RS Y-Dir** |
| | m | | mm | mm | mm | mm | % | % |
| Story6 | 18 | Top | 6.439 | 6.13 | 11.175 | 10.393 | 57.619 | 58.982 |
| Story5 | 15 | Top | 5.248 | 4.944 | 9.077 | 8.352 | 57.816 | 59.195 |
| Story4 | 12 | Top | 3.985 | 3.709 | 6.864 | 6.236 | 58.056 | 59.477 |
| Story3 | 9 | Top | 2.715 | 2.492 | 4.66 | 4.169 | 58.261 | 59.774 |
| Story2 | 6 | Top | 1.538 | 1.385 | 2.634 | 2.309 | 58.390 | 59.982 |
| Story1 | 3 | Top | 0.575 | 0.504 | 0.986 | 0.839 | 58.316 | 60.071 |
| Base | 0 | Top | 0 | 0 | 0 | 0 | 0 | 0 |

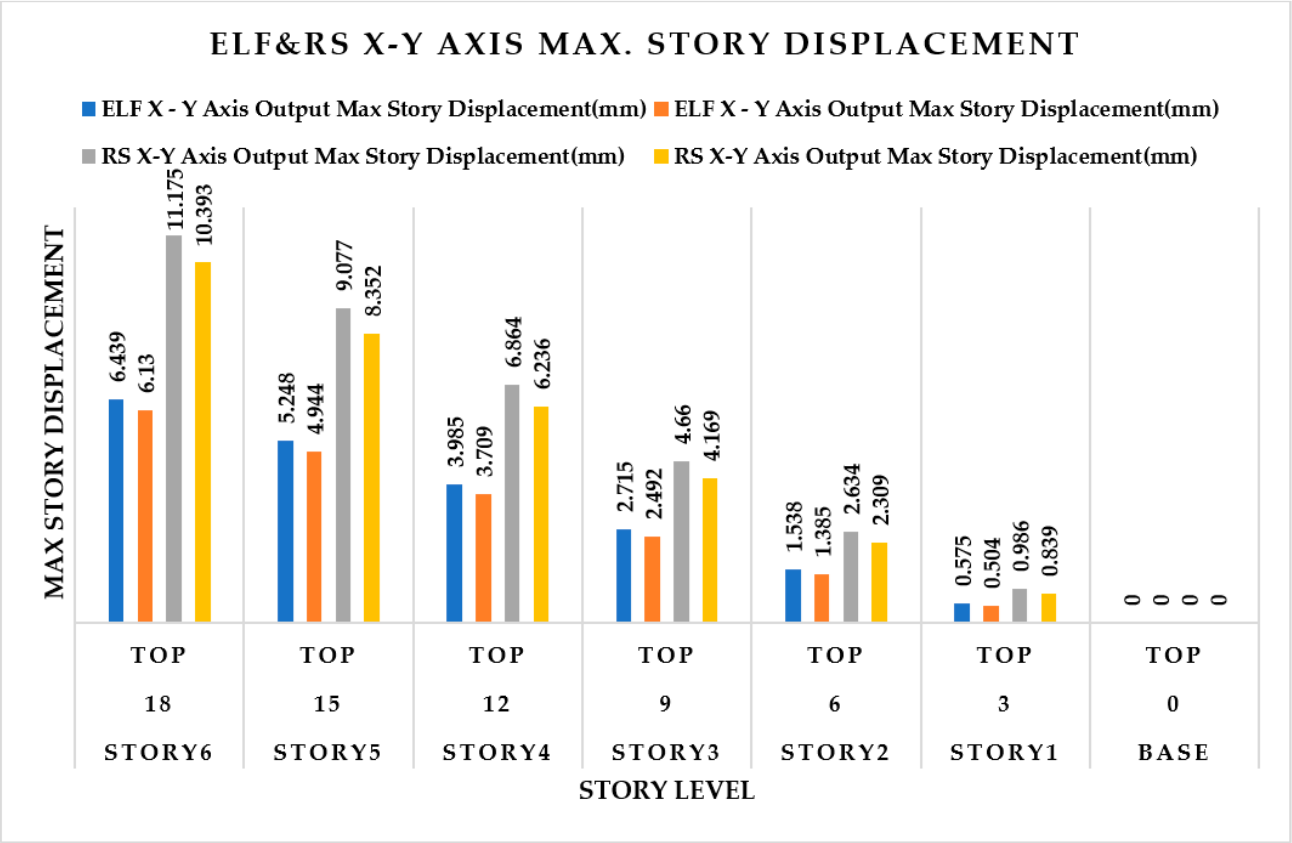


**Figure 12.** ELF and RS X-Y axis max story displacement.

Table 12, Figures A14b, A18a, A22b and 13 illustrate the six-story max story drifts by dynamically and statically analyzing the sample structure results. It can be seen that the maximum MSD obtained by RS is higher than that obtained by ELF for all the stories. The ELF result indicated 58.35% in the X-axis and 60% in the Y-axis of the RS results. It can be observed that the difference in MSD generated by both methods decreases from the bottom to the top of the structure in both X and Y directions.

**Table 12.** A comparison of static and dynamic analysis results in max story drifts for six-story structures.

| | | | ELF X-Y Axis Output | | RS X-Y Axis Output | | X-Y Axis Output | |
|---|---|---|---|---|---|---|---|---|
| | | | Max. Story Drifts | | Max. Story Drifts | | Max. Story Drifts | |
| Story | Elevation | Location | X-Dir | Y-Dir | X-Dir | Y-Dir | ELF vs. RS X-Dir | ELF vs. RS Y-Dir |
| | m | | | | | | % | % |
| Story6 | 18 | Top | 0.000397 | 0.000395 | 0.000705 | 0.000685 | 56.312 | 57.664 |
| Story5 | 15 | Top | 0.000421 | 0.000412 | 0.000745 | 0.000711 | 56.510 | 57.946 |
| Story4 | 12 | Top | 0.000423 | 0.000406 | 0.000741 | 0.000694 | 57.085 | 58.501 |
| Story3 | 9 | Top | 0.000392 | 0.000369 | 0.000679 | 0.000623 | 57.731 | 59.229 |
| Story2 | 6 | Top | 0.000321 | 0.000294 | 0.000551 | 0.000491 | 58.257 | 59.877 |
| Story1 | 3 | Top | 0.000192 | 0.000168 | 0.000329 | 0.00028 | 58.358 | 60 |
| Base | 0 | Top | 0 | 0 | 0 | 0 | 0 | 0 |

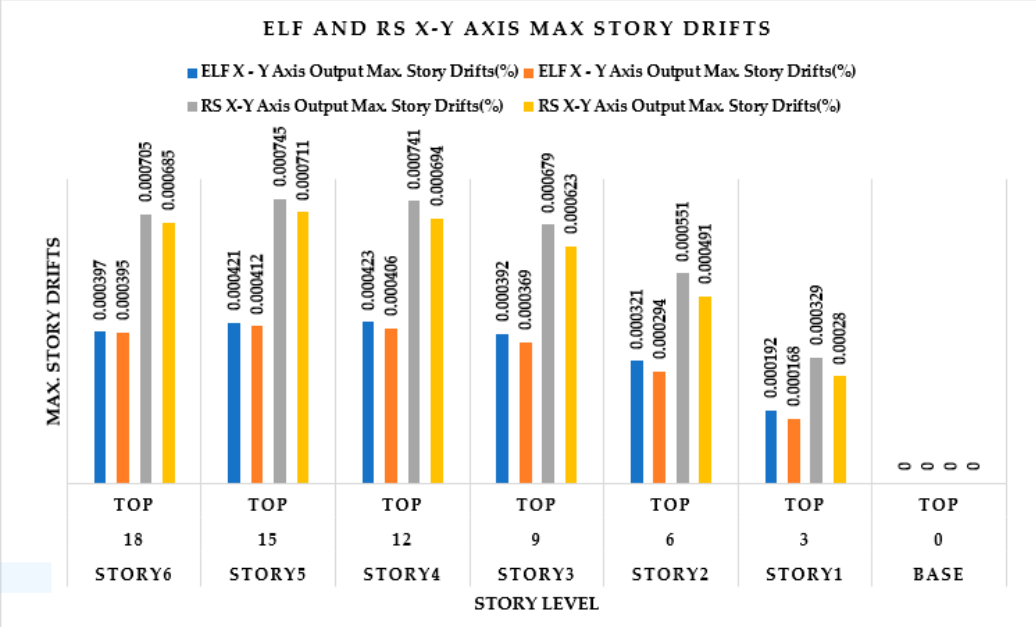


**Figure 13.** ELF and RS X-Y axis max story drifts.

A comparison of the static and dynamic analysis results in story shears for six-story structures in Figures A14a, A19a, A21b and 14 illustrates the six-story max story shear by dynamically and statically analyzing the sample structure results. It can be seen that the maximum MSD obtained by RS is higher than that obtained by ELF for the whole story. The ELF result indicated 59.51% in the X-axis and 59.42% in the Y-axis of the RS results. It can be observed that the difference in MSD generated by both methods decreases from the bottom to the top of the structure in both X and Y directions.

Table 13, Figures A15a, A18b, A23a and 15 illustrate the six-story max overturning moment by dynamically and statically analyzing the sample structure results. It can be seen that the maximum MOM obtained by RS is higher than that obtained by ELF for the whole story. The ELF result indicated 60.03% in the X-axis and 60.23% in the Y-axis of the RS results. It can be observed that the difference in MOM generated by both methods decreases from the bottom to the top of the structure in both X and Y directions.

**Table 13.** Comparison of static and dynamic analysis results for overturning moment for six-story structures.

| | | | **ELF X-Y Axis Output** | | **RS X-Y Axis Output** | | **X-Y Axis Output** | |
|---|---|---|---|---|---|---|---|---|
| | | | **Overturning Moment** | | **Overturning Moment** | | **Overturning Moment** | |
| **Story** | **Elevation** | **Location** | **X-Dir** | **Y-Dir** | **X-Dir** | **Y-Dir** | **ELF vs. RS X-Dir** | **ELF vs. RS Y-Dir** |
| | m | | kN-m | kN-m | kN-m | kN-m | % | % |
| Story6 | 18 | Top | 0 | 0 | 0 | 0 | 0 | 0 |
| Story5 | 15 | Top | 9514.703 | −9514.7029 | 19,215.76 | 18,903.87 | 49.515 | −50.332 |
| Story4 | 12 | Top | 27,574.77 | −27,574.7721 | 52,198.28 | 51,543.4 | 52.826 | −53.498 |
| Story3 | 9 | Top | 52,471.13 | −52,471.1343 | 94,172.54 | 93,324.97 | 55.718 | −56.224 |
| Story2 | 6 | Top | 82,494.72 | −82,494.7162 | 142,497.3 | 141,612.1 | 57.892 | −58.254 |
| Story1 | 3 | Top | 115,936.4 | −115,936.445 | 195,544.3 | 194,684.7 | 59.289 | −59.550 |
| Base | 0 | Top | 151,087.2 | −151,087.246 | 251,666.4 | 250,831.2 | 60.034 | −60.234 |

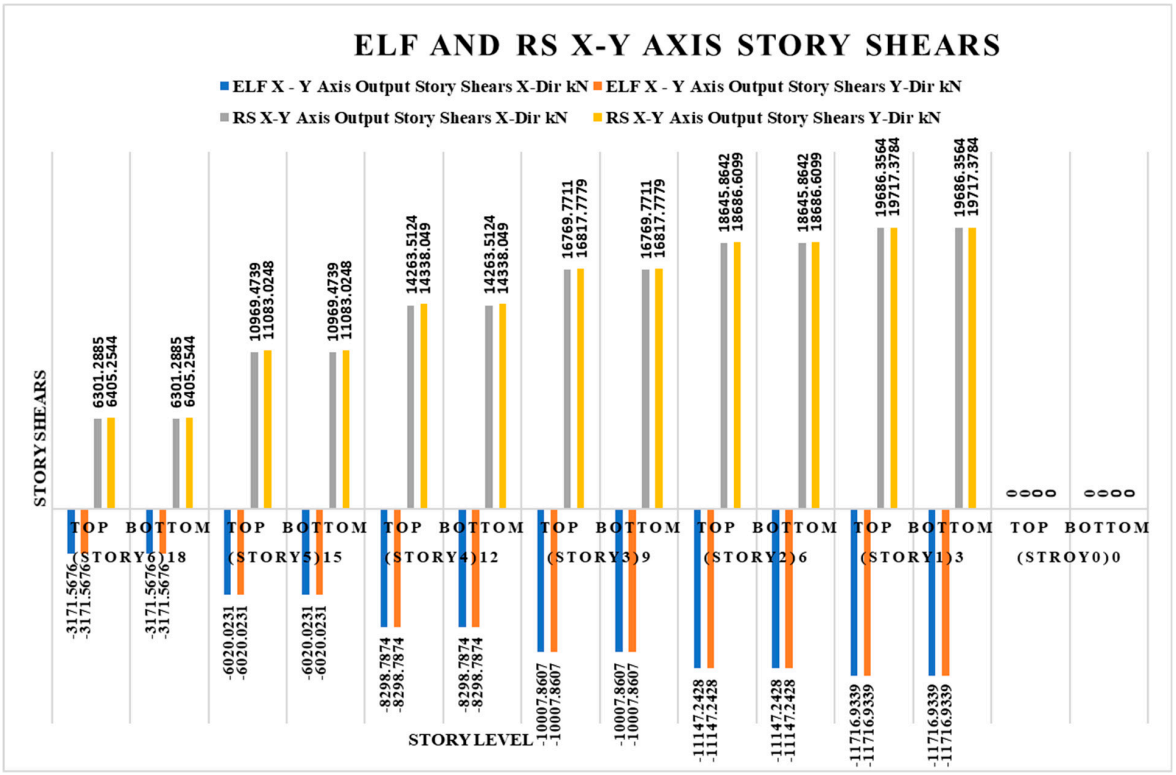


**Figure 14.** ELF and RS X-Y axis story shears.

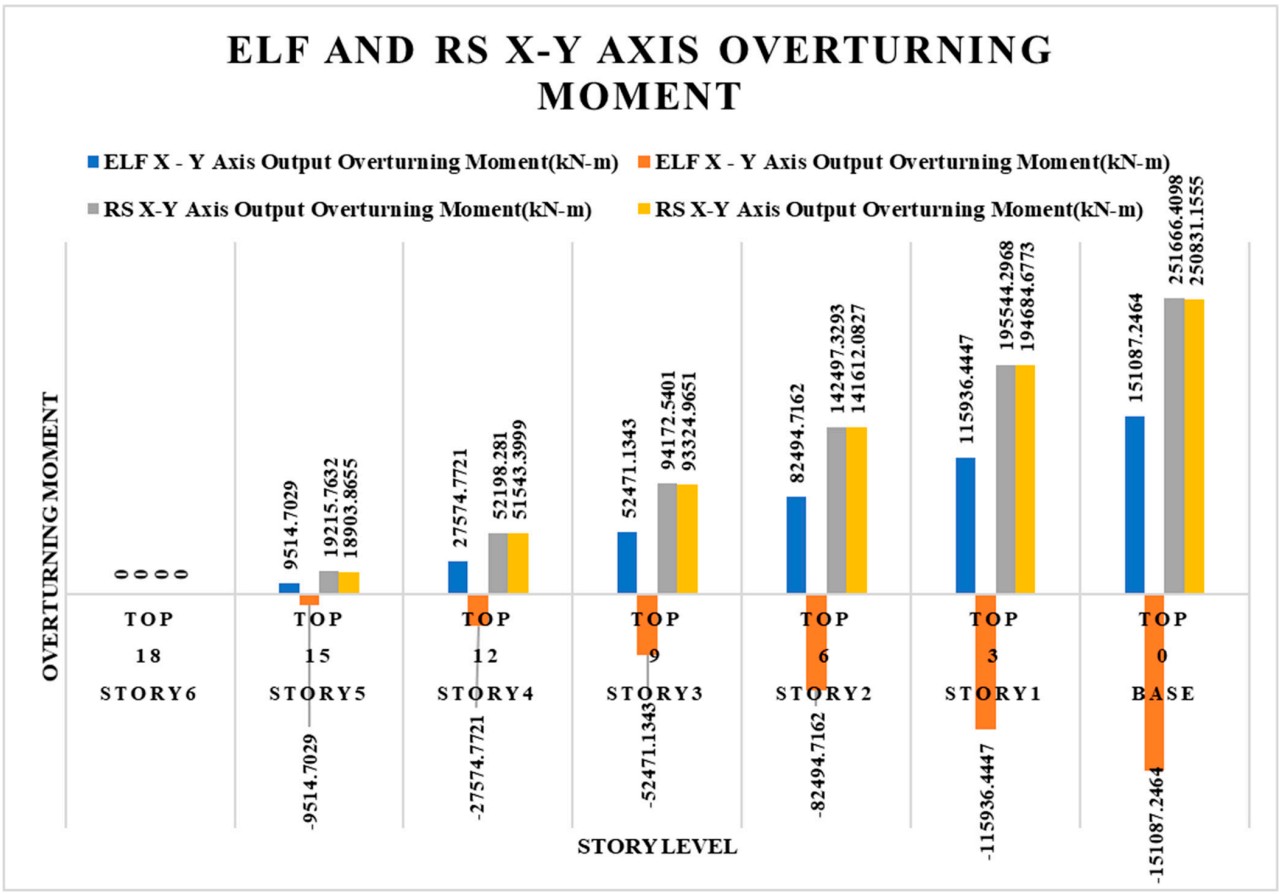


**Figure 15.** ELF and RS X-Y axis overturning moment.

Table 14, Figures A16a, A9b, A22a and 16 illustrate the six-story story stiffness by dynamically and statically analyzing the sample structure results. It can be seen that the maximum SS obtained by RS is higher than that obtained by ELF for all the stories. The ELF result indicated 98.97% in the X-axis and 98.78% in the Y-axis of the RS results. It can be observed that the difference in SS generated by both methods decreases from the bottom to the top of the structure in both X and Y directions.

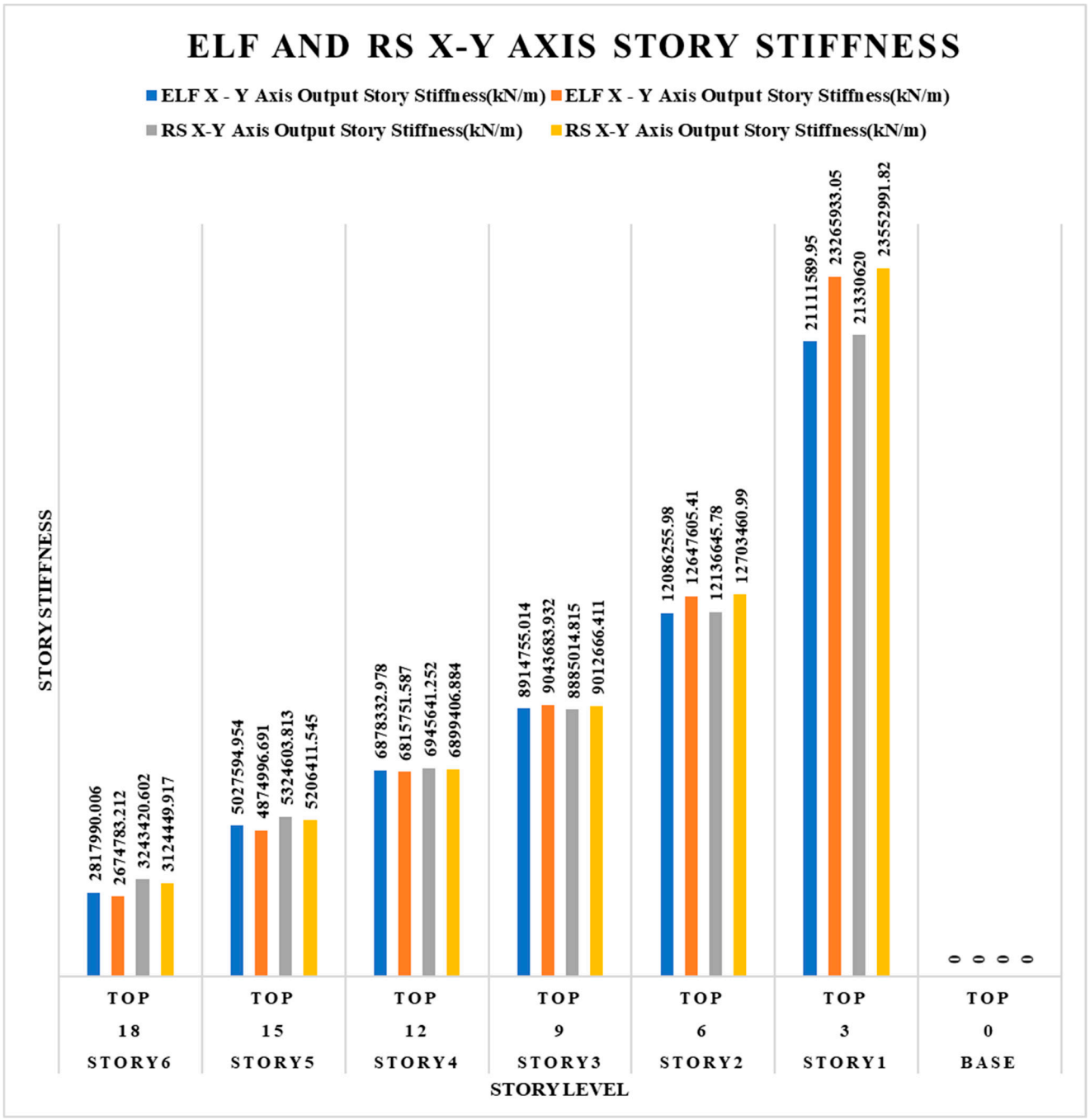


**Figure 16.** ELF and RS X-Y axis story stiffness.

**Table 14.** Comparison of static and dynamic analysis results in story stiffness for six-story structures.

| | | | ELF X-Y Axis Output | | RS X-Y Axis Output | | X-Y Axis Output | |
|---|---|---|---|---|---|---|---|---|
| | | | Story Stiffness | | Story Stiffness | | Story Stiffness | |
| Story | Elevation | Location | X-Dir | Y-Dir | X-Dir | Y-Dir | ELF vs. RS X-Dir | ELF vs. RS Y-Dir |
| | m | | kN/m | kN/m | kN/m | kN/m | % | % |
| Story6 | 18 | Top | 2,817,990 | 2,674,783.212 | 3,243,421 | 3,124,450 | 86.883 | 85.608 |
| Story5 | 15 | Top | 5,027,595 | 4,874,996.691 | 5,324,604 | 5,206,412 | 94.421 | 93.634 |
| Story4 | 12 | Top | 6,878,333 | 6,815,751.587 | 6,945,641 | 6,899,407 | 99.030 | 98.787 |
| Story3 | 9 | Top | 8,914,755 | 9,043,683.932 | 8,885,015 | 9,012,666 | 100.334 | 100.344 |
| Story2 | 6 | Top | 12,086,256 | 12,647,605.41 | 12,136,646 | 12,703,461 | 99.584 | 99.560 |
| Story1 | 3 | Top | 21,111,590 | 23,265,933.05 | 21,330,620 | 23,552,992 | 98.973 | 98.781 |
| Base | 0 | Top | 0 | 0 | 0 | 0 | 0 | 0 |

### *5.3. Twelve-Story Building*

Table 15, Figures A24a, A27b, A31a and 17 illustrate the 12-story CM displacement for diaphragm D1 by dynamically and statically analyzing the sample structure results. It can be seen that the maximum SMD obtained by RS is higher than that obtained by ELF for all the stories. The ELF result indicated 97.31% in the X-axis and 100.8997% in the Y-axis of the RS results. It can be observed that the difference in CMD generated by both methods decreases from the bottom to the top of the structure in both X and Y directions.

**Table 15.** Comparison of static and dynamic analysis results in CM displacement for diaphragm D1 for 12-story structures.

| | | | ELF X-Y Axis Output | | RS X-Y Axis Output | | X-Y Axis Output | |
|---|---|---|---|---|---|---|---|---|
| | | | CM Displacement for Diaphragm D1 | | CM Displacement for Diaphragm D1 | | CM Displacement for Diaphragm D1 | |
| Story | Elevation | Location | X-Dir | Y-Dir | X-Dir | Y-Dir | ELF vs. RS X-Dir | ELF vs. RS Y-Dir |
| | m | | mm | mm | mm | mm | % | % |
| Story12 | 36 | Top | 35.003 | 36.847 | 30.282 | 31.18 | 115.590 | 118.175 |
| Story11 | 33 | Top | 31.577 | 33.133 | 27.213 | 27.938 | 116.036 | 118.594 |
| Story10 | 30 | Top | 28.069 | 29.347 | 24.103 | 24.663 | 116.454 | 118.992 |
| Story9 | 27 | Top | 24.497 | 25.514 | 20.987 | 21.394 | 116.724 | 119.257 |
| Story8 | 24 | Top | 20.895 | 21.668 | 17.902 | 18.169 | 116.718 | 119.258 |
| Story7 | 21 | Top | 17.313 | 17.865 | 14.888 | 15.028 | 116.288 | 118.878 |
| Story6 | 18 | Top | 13.817 | 14.174 | 11.982 | 12.01 | 115.314 | 118.018 |
| Story5 | 15 | Top | 10.486 | 10.678 | 9.221 | 9.159 | 113.718 | 116.584 |
| Story4 | 12 | Top | 7.412 | 7.475 | 6.651 | 6.528 | 111.441 | 114.506 |
| Story3 | 9 | Top | 4.697 | 4.675 | 4.336 | 4.188 | 108.325 | 111.628 |
| Story2 | 6 | Top | 2.461 | 2.401 | 2.365 | 2.231 | 104.059 | 107.619 |
| Story1 | 3 | Top | 0.833 | 0.785 | 0.856 | 0.778 | 97.3130 | 100.899 |
| Base | 0 | Top | 0 | 0 | 0 | 0 | 0 | 0 |

The comparison of the static and dynamic analysis results of drifts for diaphragm D1 for 12-story structures in Figures A24b, A28a, A31b and 18 illustrates the 12-story drift for diaphragm D1 by dynamically and statically analyzing the sample structure results. It can be seen that the maximum DFD obtained by RS is higher than that obtained by ELF for all the stories. The ELF result indicated 93.83% in the X-axis and 100.3831% in the Y-axis of the RS results. It can be observed that the difference in DFD generated by both methods decreases from the bottom to the top of the structure in both X and Y directions.

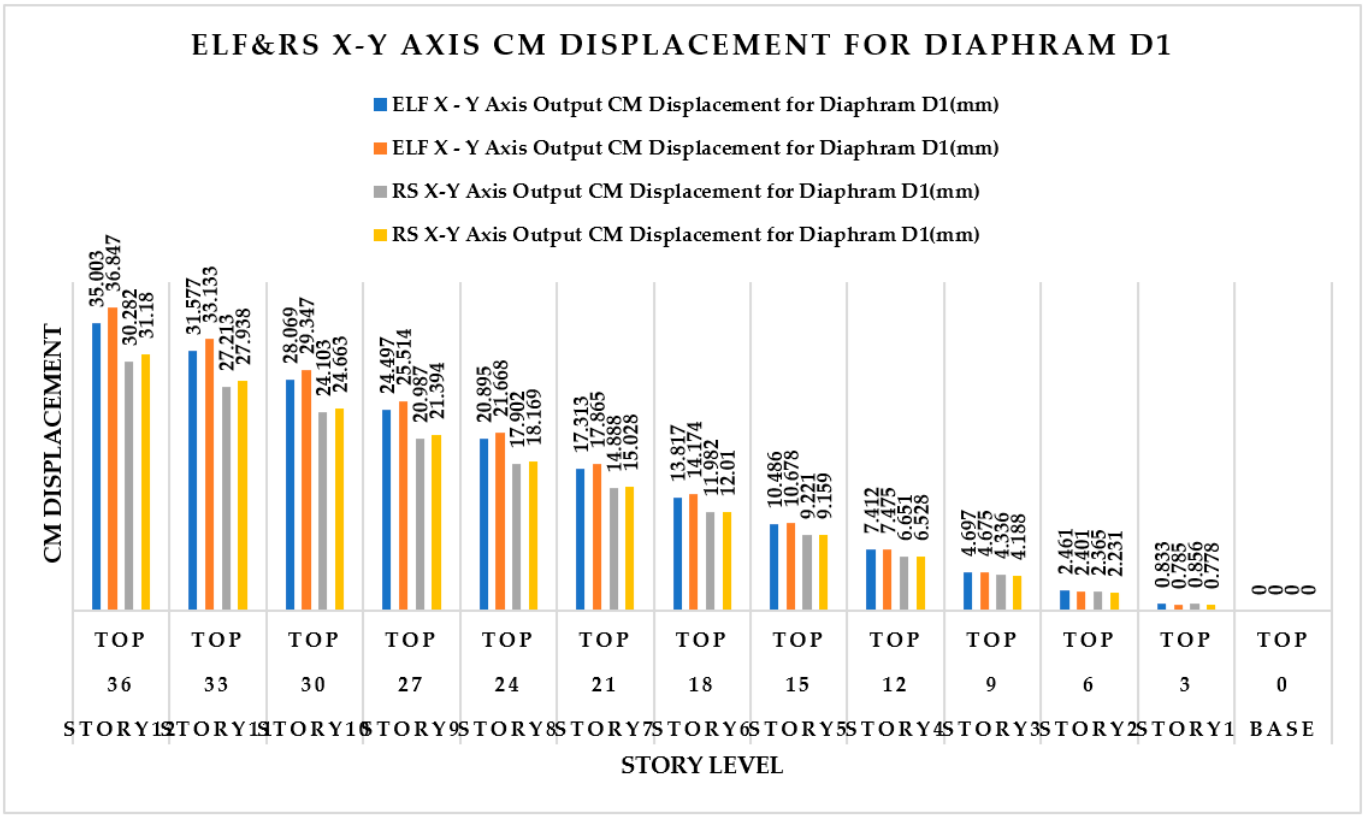


**Figure 17.** ELF and RS X-Y axis CM displacement for diaphragm D1.

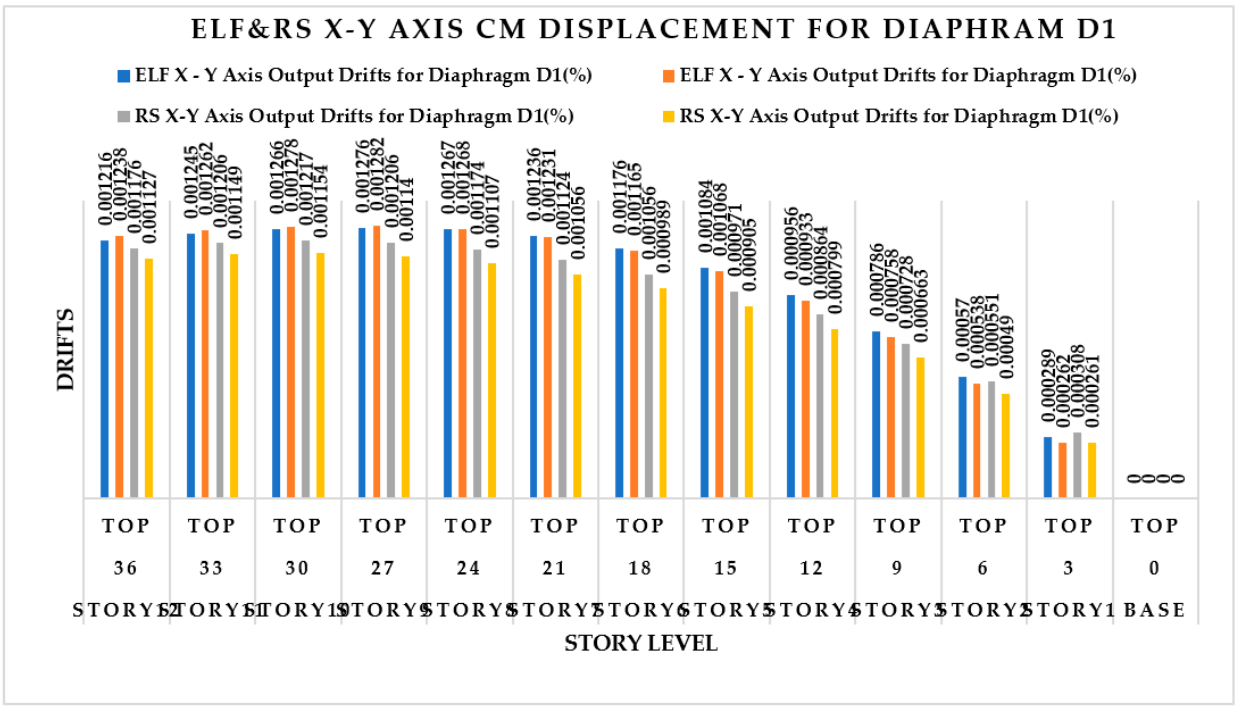


**Figure 18.** ELF and RS axis drifts.

The comparison of the static and dynamic analysis results of max story displacement for 12-story structures in Figures A25a, A28b, A32a and 19 illustrates the 12-story max story displacement by dynamically and statically analyzing the sample structure results. It can

be seen that the maximum MSD obtained by RS is higher than that obtained by ELF for the whole story. The ELF result indicated 94.04% in the X-axis and 100.2554% in the Y-axis of the RS results. It can be observed that the difference in MSD generated by both methods decreases from the bottom to the top of the structure in both X and Y directions.

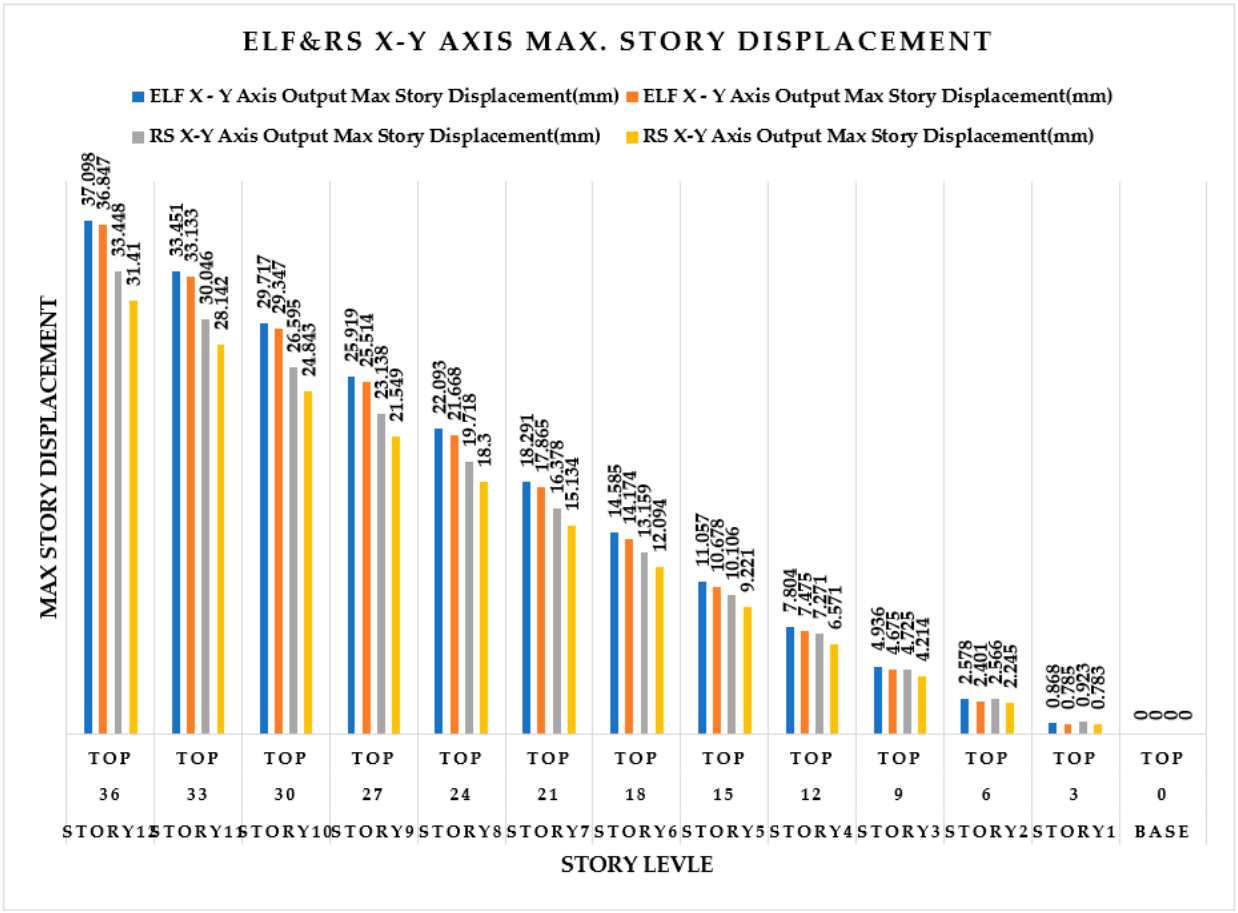


**Figure 19.** ELF and RS X-Y axis max story displacement.

The comparison of the static and dynamic analysis results of max story drifts for 12-story structures in Figures A25b, A29a, A32b and 20 illustrates the 12-story max story drifts by dynamically and statically analyzing the sample structure results. It can be seen that the maximum MSD obtained by RS is higher than that obtained by ELF for the whole story. The ELF result indicated 93.83% in the X-axis and 100.38% in the Y-axis of the RS results. It can be observed that the difference in MSD generated by both methods decreases from the bottom to the top of the structure in both X and Y directions.

The comparison of static and dynamic analysis results of story shears for 12-story structures in Figures A26b, A30a, A34 and 21 illustrates the 12-story max story shear by dynamically and statically analyzing the sample structure results. It can be seen that the maximum MSD obtained by RS is higher than that obtained by ELF for the whole story. The ELF result indicated 79.98% in the X-axis and 80.08% in the Y-axis of the RS results. It can be observed that the difference in MSD generated by both methods decreases from the bottom to the top of the structure in both X and Y directions.

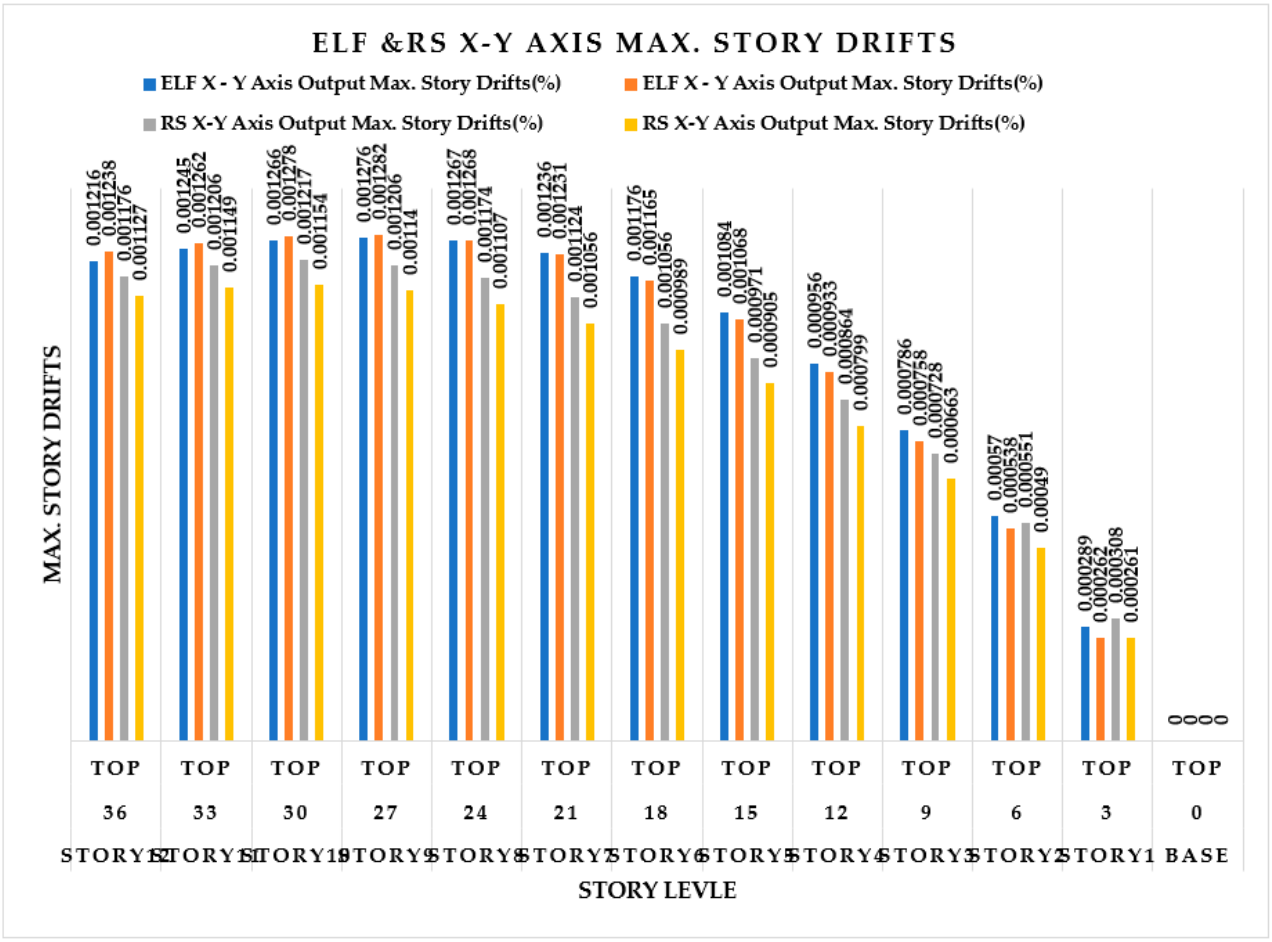


**Figure 20.** ELF and RS X-Y axis max story drifts.

The comparison of the static and dynamic analysis results of the overturning moment for 12-story structures in Figures A26a, A29b, A33a and 22 illustrates the 12-story max overturning moment by dynamically and statically analyzing the sample structure results. It can be seen that the maximum MOM obtained by RS is higher than that obtained by ELF for all the stories. The ELF result indicated 116.83% in the X-axis and 115.34% in the Y-axis of the RS results. It can be observed that the difference in MOM generated by both methods decreases from the bottom to the top of the structure in both X and Y directions.

The comparison of the static and dynamic analysis results of story stiffness for 12-story structures in Figures A27a, A30b, A33b and 23 illustrates the 12-story story stiffness by dynamically and statically analyzing the sample structure results. It can be seen that the maximum SS obtained by RS is higher than ELF for all the stories. The ELF result indicated 82.32% in the X-axis and 79.62% in the Y-axis of the RS results. It can be observed that the difference in SS generated by both methods decreases from the bottom to the top of the structure in both X and Y directions.

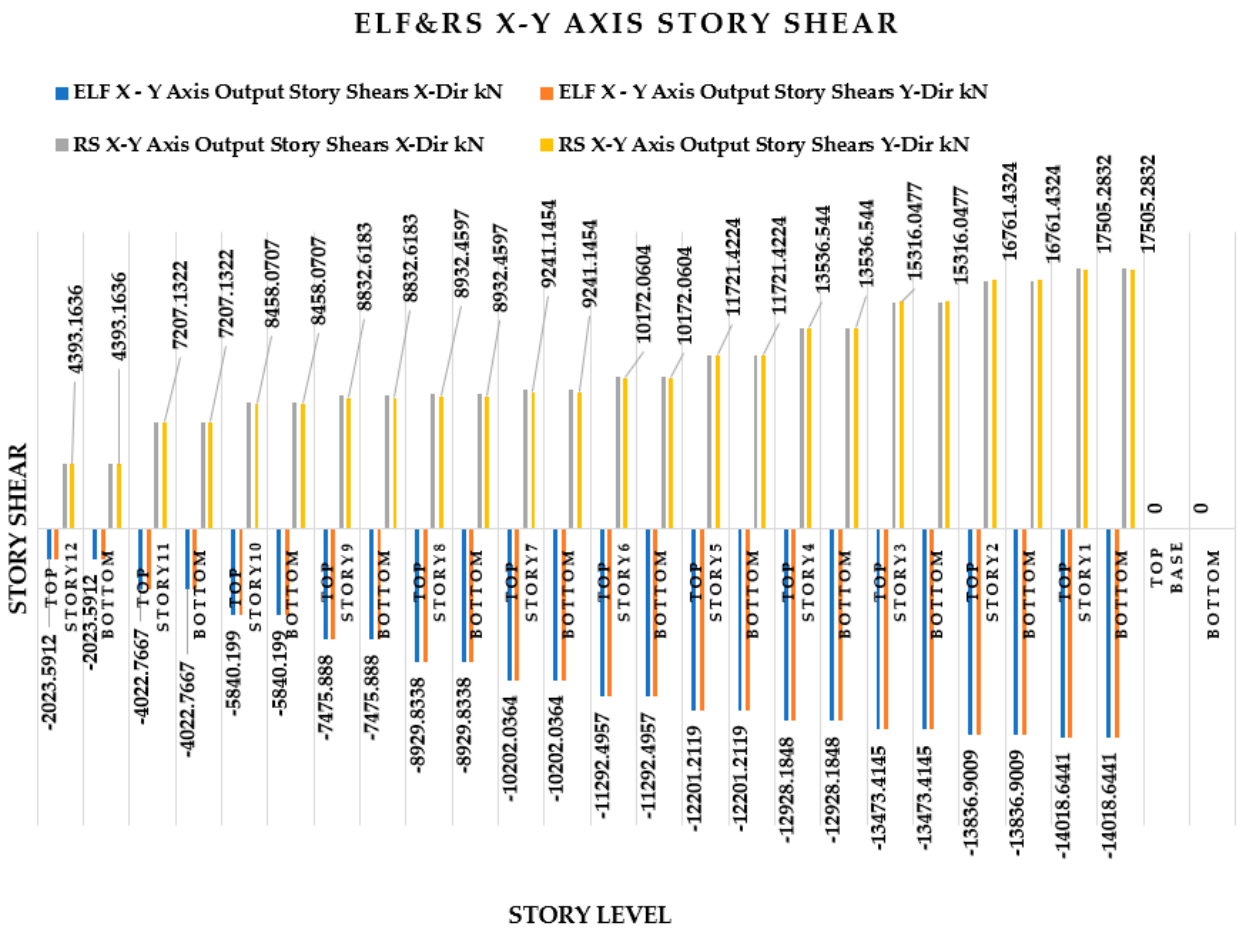


**Figure 21.** ELF and RS X-Y axis story shears.

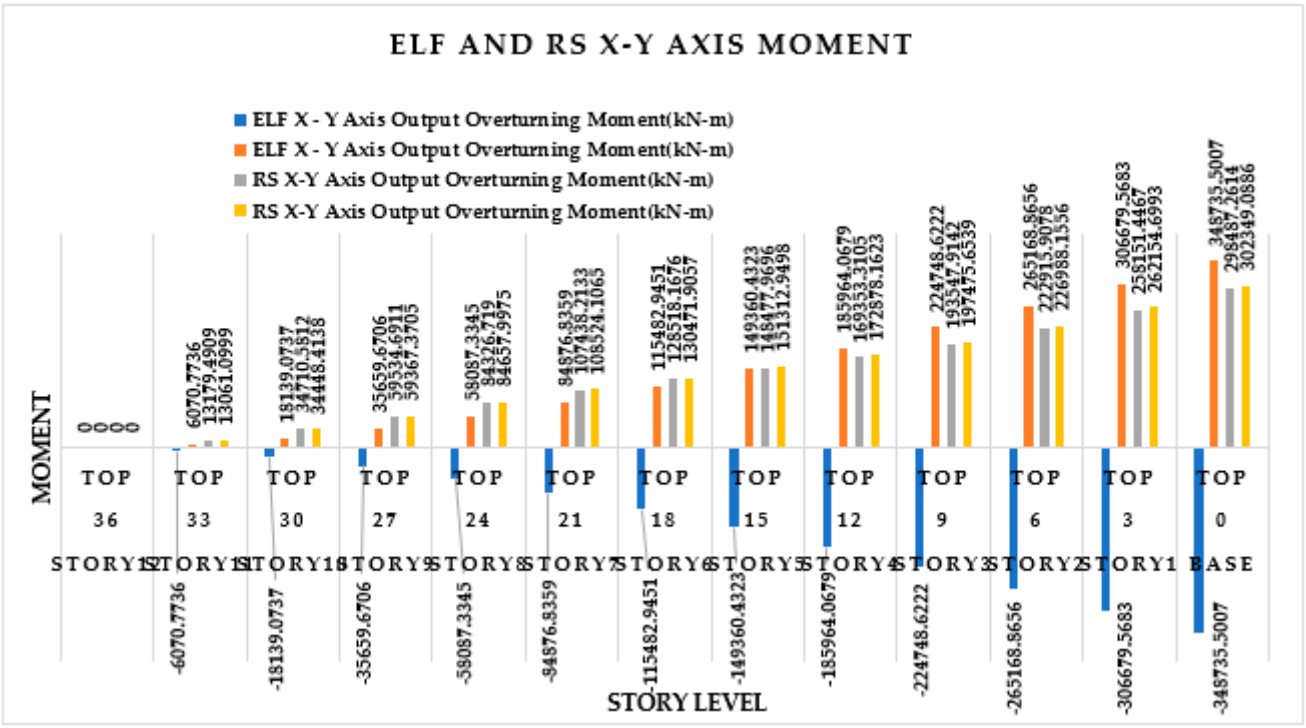


**Figure 22.** ELF and RS X-Y axis overturning moment.

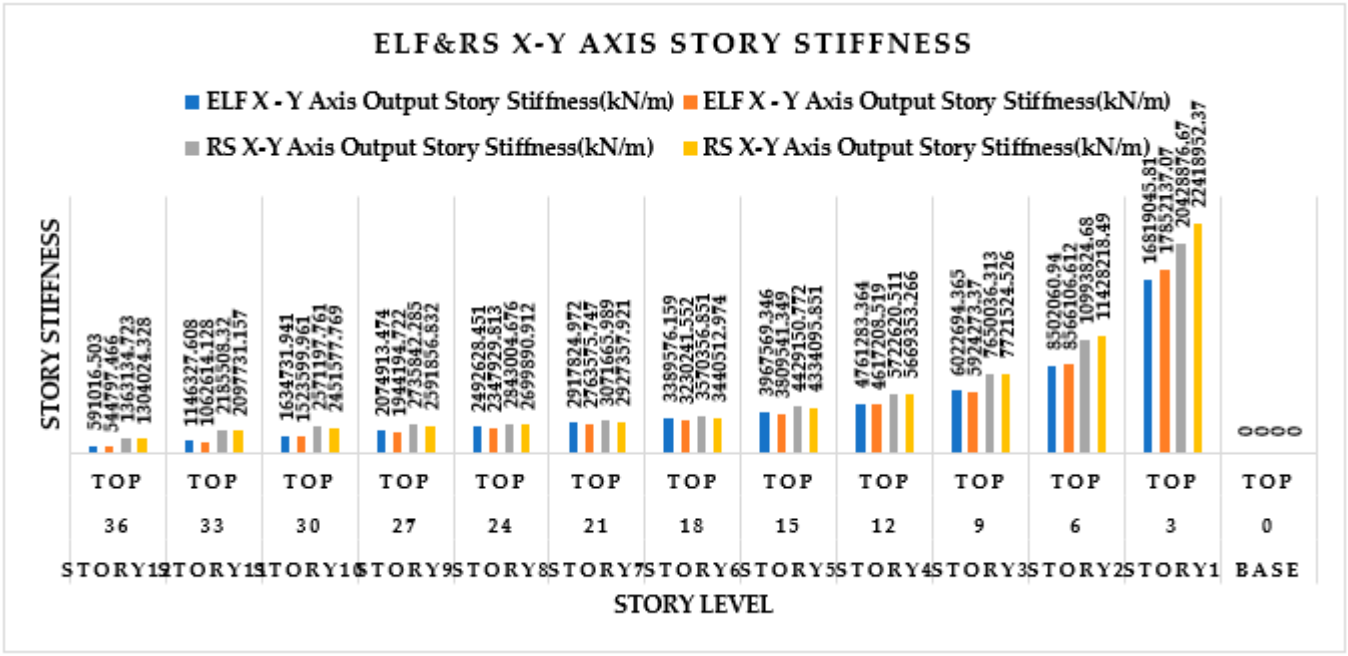


**Figure 23.** ELF and RS X-Y axis story stiffness.

### *5.4. Eighteen-Story Building*

Figures A35a, A38b and A42a illustrate the 18-story CM displacement for diaphragm D1 by dynamically and statically analyzing the sample structure results. It can be seen that the maximum SMD obtained by RS is higher than that obtained by ELF for all the stories. The ELF result indicated 123.87% in the X-axis and 129.35% in the Y-axis of the RS results. It can be observed that the difference in CMD generated by both methods decreases from the bottom to the top of the structure in both X and Y directions.

Figures A35b, A39a and A42b illustrate the 18-story drift for diaphragm D1 by dynamically and statically analyzing the sample structure results. It can be seen that the maximum DFD obtained by RS is higher than ELF for the whole story. The ELF result indicated 119.4% in the X-axis and 128.68% in the Y-axis of the RS results. It can be observed that the difference in DFD generated by both methods decreases from the bottom to the top of the structure in both X and Y directions.

Figures A36b, A39b and A43a illustrate the 18-story max story displacement by dynamically and statically analyzing the sample structure results. It can be seen that the maximum MSD obtained by RS is higher than that obtained by ELF for the whole story. The ELF result indicated 119.539% in the X-axis and 128.51% in the Y-axis of the RS results. It can be observed that the difference in MSD generated by both methods decreases from the bottom to the top of the structure in both X and Y directions.

Figures A36a, A40a and A43b illustrate the 18-story max story drifts by dynamically and statically analyzing the sample structure results. It can be seen that the maximum MSD obtained by RS is higher than that obtained by ELF for all the stories. The ELF result indicated 119.407% in the X-axis and 128.68% in the Y-axis of the RS results. It can be observed that the difference in MSD generated by both methods decreases from the bottom to the top of the structure in both X and Y directions.

Figures A37b, A41a and A44b illustrate the 18-story max story shear by dynamically and statically analyzing sample structure results. It can be seen that the maximum MSD obtained by RS is higher than that obtained by ELF for all the stories. The ELF result indicated 97.09% in the X-axis and 36.05% in the Y-axis of the RS results. It can be observed that the difference in MSD generated by both methods decreases from the bottom to the top of the structure in both X and Y directions.

Figures A37a, A40b and A44a illustrate the 18-story max overturning moment by dynamically and statically analyzing the sample structure results. It can be seen that the maximum MOM obtained by RS is higher than that obtained by ELF for the whole story. The ELF result indicated 157.115% in the X-axis and 154.47% in the Y-axis of the RS results. It can be observed that the difference in MOM generated by both methods decreases from the bottom to the top of the structure in both X and Y directions.

Figures A38a, A41b and A45a illustrate the 18-story story stiffness by dynamically and statically analyzing the sample structure results. It can be seen that the maximum SS obtained by RS is higher than ELF for the whole story. The ELF result indicated 78.53% on the X-axis and 76.07% on the Y-axis of the RS results. It can be observed that the difference in SS generated by both methods decreases from the bottom to the top of the structure in both X and Y directions.

## 6. Conclusions

From the extensive data, we concluded that the CM displacement for diaphragm D1 for a three-story structure by static and dynamic analysis shows that the maximum SMD obtained by RS is higher than that obtained by ELF for all the stories. The ELF results indicated 73.188% in the X-axis and 73.44% in the Y-axis of the RS results. We concluded that CM drifts for diaphragm D1 for a three-story structure by static and dynamic analysis show that the maximum DFD obtained by RS is higher than ELF for the whole story. The ELF results indicated 71.97% in the X-axis and 73.82% in the Y-axis of the RS results. In addition, it has been concluded that the max story displacement for a three-story structure by static and dynamic analysis shows that the maximum MSD obtained by RS is higher than that obtained by ELF for all stories. The ELF results indicated 71.92% in the X-axis and 74.04% in the Y-axis of the RS results. From the extensive data, we concluded that max story drifts for a three-story structure by static and dynamic analysis show that the MSD obtained by RS is higher than ELF for the whole story. The ELF results indicated 71.97% in the X-axis and 73.82% in the Y-axis of the RS results. From the extensive data, we concluded that max story shears for a three-story structure by static and dynamic analysis show that the MSD obtained by RS is higher than ELF for the whole story. The ELF results indicated 73.68% in the X-axis and 74.20% in the Y-axis of RS. From the extensive and wide range of data, we concluded that the overturning moment for a three-story structure by static and dynamic analysis shows that the MOM obtained by RS is higher than ELF for the whole story. The ELF results indicated 73.75% on the X-axis and 73.56% on the Y-axis of the RS results.

From extensive data, it can be concluded that CM displacement for diaphragm D1 for a six-story structure by static and dynamic analysis shows that the maximum SMD obtained by RS is higher than that obtained by ELF for all the stories. The ELF results indicated 60.19% in the X-axis and 60.35% in the Y-axis of the RS results. We concluded that CM drifts for diaphragm D1 for a six-story structure by static and dynamic analysis show that the maximum DFD obtained by RS is higher than ELF for the whole story. The ELF results indicated 59.38% in the X-axis and 60% in the Y-axis of the RS results. In addition, we concluded that max story displacement for a six-story structure by static and dynamic analysis shows that the maximum MSD obtained by RS is higher than that obtained by ELF for all stories. The ELF results indicated 58.31% in the X-axis and 60% in the Y-axis of the RS results. From the extensive data, we concluded that the max story drifts for a six-story structure by static and dynamic analysis show that the MSD obtained by RS is higher than ELF for the whole story. The ELF results indicated 58.35% in the X-axis and 60% in the Y-axis of the RS results. From the extensive data, we concluded that max story shears for a six-story structure by static and dynamic analysis show that the MSD obtained by RS is higher than ELF for the whole story. The ELF results indicated 59.51% in the X-axis and 59.42% in the Y-axis of the RS results. From the extensive and wide range of data, we concluded that the overturning moment for a six-story structure by static and dynamic

analysis shows that the MOM obtained by RS is higher than ELF for the whole story. The ELF results indicated 60.03% in the X-axis and 60.23% in the Y-axis of the RS results.

From the extensive data, we concluded that CM displacement for diaphragm D1 for a 12-story structure by static and dynamic analysis shows that the maximum SMD obtained by RS is higher than that obtained by ELF for all the stories. The ELF results indicated 97.31% in the X-axis and 100.8997% in the Y-axis of the RS results. We concluded that CM drifts for diaphragm D1 for a 12-story structure by static and dynamic analysis show that the maximum DFD obtained by RS is higher than ELF for the whole story. The ELF results indicated 93.83% in the X-axis and 100.3831% in the Y-axis of the RS results. In addition, we concluded that the max story displacement for a 12-story structure by static and dynamic analysis shows that the maximum MSD obtained by RS is higher than that obtained by ELF for all stories. The ELF results indicated 94.04% in the X-axis and 100.2554% in the Y-axis of the RS results. From the extensive data, we concluded that max story drifts for a 12-story structure by static and dynamic analysis show that the MSD obtained by RS is higher than ELF for the whole story. The ELF results indicated 93.83% in the X-axis and 100.38% in the Y-axis of the RS results. From the extensive and wide range of data, we concluded that max story shears for a 12-story structure by static and dynamic analysis show that the MSD obtained by RS is higher than ELF for the whole story. The ELF results indicated 79.98% in the X-axis and 80.08% in the Y-axis of the RS results. From the extensive and wide range of data, we concluded that the overturning moment for a 12-story structure by static and dynamic analysis shows that the MOM obtained by RS is higher than ELF for the whole story. The ELF results indicated 116.83% in the X-axis and 115.34% in the Y-axis of the RS results.

From the extensive and wide range of data, we concluded that CM displacement for diaphragm D1 for an 18-story structure by static and dynamic analysis shows that the maximum SMD obtained by RS is higher than that obtained by ELF for all the stories. The ELF results indicated 123.87% in the X-axis and 129.35% in the Y-axis of the RS results. We concluded that CM drifts for diaphragm D1 for an 18-story structure by static and dynamic analysis show that the maximum DFD obtained by RS is higher than ELF for the whole story. The ELF results indicated 119.4% in the X-axis and 128.68% in the Y-axis of the RS results.

In addition, we concluded that the max story displacement for an 18-story structure by static and dynamic analysis shows that the maximum MSD obtained by RS is higher than that obtained by ELF for all stories. The ELF results indicated 119.539% in the X-axis and 128.51% in the Y-axis of the RS results. From the extensive data, we concluded that max story drifts for an 18-story structure by static and dynamic analysis show that the MSD obtained by RS is higher than ELF for the whole story. The ELF results indicated 119.407% in the X-axis and 128.68% in the Y-axis of the RS results. From the extensive data, we concluded that the max story shears for an 18-story structure by static and dynamic analysis show that the MSD obtained by RS is higher than the ELF for the whole story. The ELF results indicated 97.09% in the X-axis and 36.05% in the Y-axis of the RS results. From the extensive and wide range of data, we concluded that the overturning moment for an 18-story structure by static and dynamic analysis shows that the MOM obtained by RS is higher than the ELF for the whole story. The ELF results indicated 115.115% in the X-axis and 154.47% in the Y-axis of the RS results.

According to the research findings, response spectrum analysis emerges as a crucial dynamic method, offering superior results without requiring extensive modeling compared to static analysis. While engineers and researchers generally favor RS analysis over ELF for its accuracy, it is essential to acknowledge its limitations, as it relies solely on linear elastic analysis. Advanced dynamic analysis tools like non-linear time–history analysis can be employed to produce more precise results despite being more complex and time-consuming. For practical applications, utilizing dynamic analysis (RS) is recommended over static analysis (ELF), especially in high-rise structures, as it delivers comparable outcomes with less computational effort, ensuring a cost-effective and safe design.

**Author Contributions:** Conceptualization, V.W.Y.T., A.C.J.E., and M.A.; methodology, V.W.Y.T., A.C.J.E., and M.A.; software, M.A.; validation, formal analysis, V.W.Y.T., A.C.J.E., and M.A.; investigation, V.W.Y.T., A.C.J.E., and M.A.; resources, V.W.Y.T., A.C.J.E., and M.A.; data curation, V.W.Y.T., A.C.J.E., and M.A.; writing—original draft preparation, M.A.; writing—review and editing, V.W.Y.T., A.C.J.E., and M.A.; visualization, V.W.Y.T., A.C.J.E., and M.A.; supervision, V.W.Y.T., A.C.J.E., and M.A.; project administration, V.W.Y.T., A.C.J.E., and M.A. All authors have read and agreed to the published version of the manuscript.

**Funding:** This research received no external funding.

**Data Availability Statement:** The data showcased in this study can be obtained upon request from the corresponding author. However, please note that the data are not publicly accessible in compliance with EIT's privacy policy.

**Acknowledgments:** The authors express their heartfelt appreciation to the Engineering Institute of Technology for their invaluable support.

**Conflicts of Interest:** The authors assert that there are no conflicts of interest to disclose.

## Appendix A

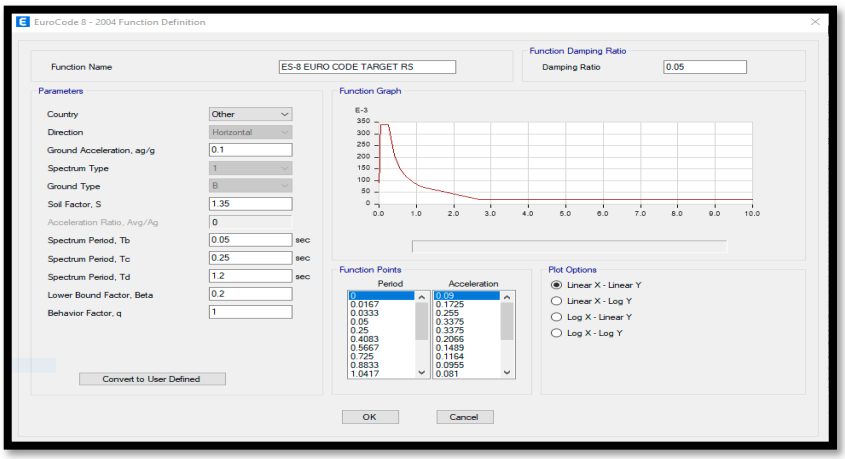


**Figure A1.** Target response spectrum as per ES EN 1998-1:2015 [54].

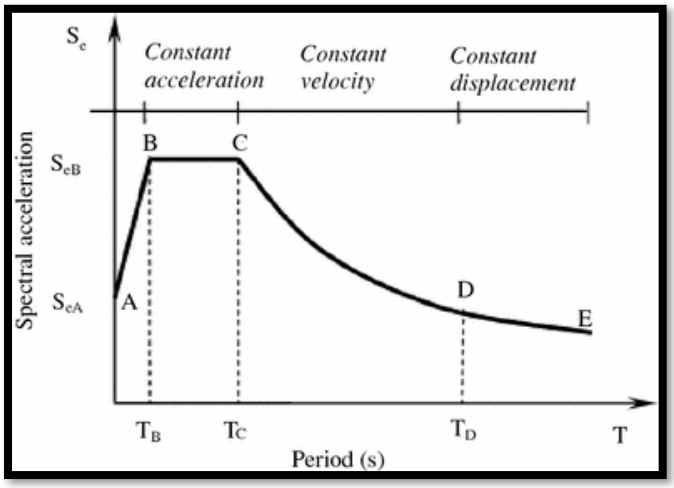


**Figure A2.** Shape of the elastic response spectrum as per ES EN 1998-1:2015.

**Table A1.** Elastic response spectra as per ES EN 1998-1:2015.

| Ground Type | S | $T_B$ (S) | $T_C$ (S) | $T_D$ (S) |
|---|---|---|---|---|
| A | 1.0 | 0.05 | 0.25 | 1.2 |
| B | 1.35 | 0.05 | 0.25 | 1.2 |
| C | 1.5 | 0.10 | 0.25 | 1.2 |
| D | 1.8 | 0.10 | 0.30 | 1.2 |
| E | 1.6 | 0.05 | 0.25 | 1.2 |

**Table A2.** Values of the parameters describing the recommended Type II elastic response spectra as per ES EN 1998-1:2015.

| Ground Type | S | $T_B$ (S) | $T_C$ (S) | $T_D$ (S) |
|---|---|---|---|---|
| A | 1.0 | 0.15 | 0.4 | 2.0 |
| B | 1.2 | 0.15 | 0.5 | 2.0 |
| C | 1.15 | 0.20 | 0.6 | 2.0 |
| D | 1.35 | 0.20 | 0.8 | 2.0 |
| E | 1.4 | 0.15 | 0.5 | 2.0 |

## Appendix B

ETABS output result.

Three-story sample RC building ETABS output.

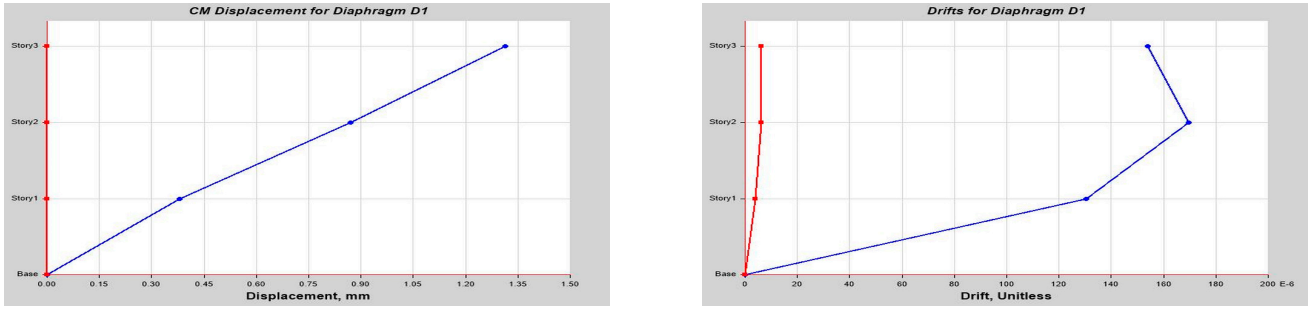


(**a**) (**b**)

**Figure A3.** (**a**) CM displacement for diaphragm D1 (X-axis); (**b**) drift for diaphragm D1 (X-axis).

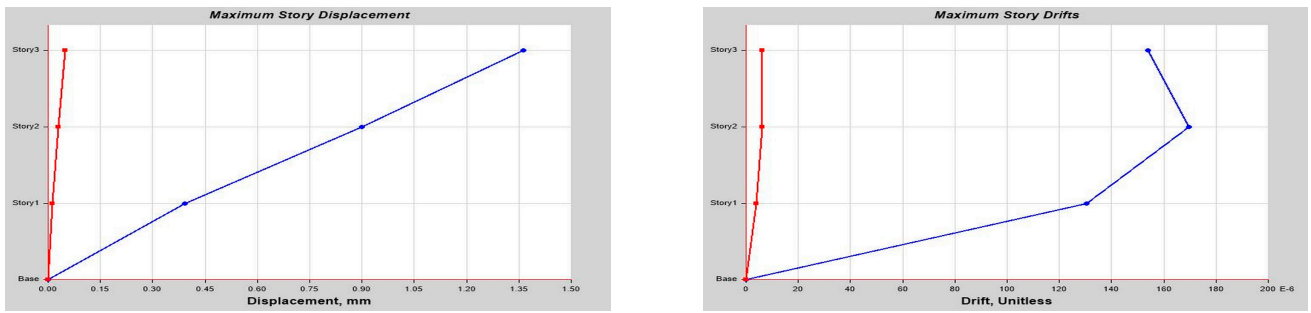


(**a**) (**b**)

**Figure A4.** (**a**) Maximum story displacement; (**b**) maximum story drifts.

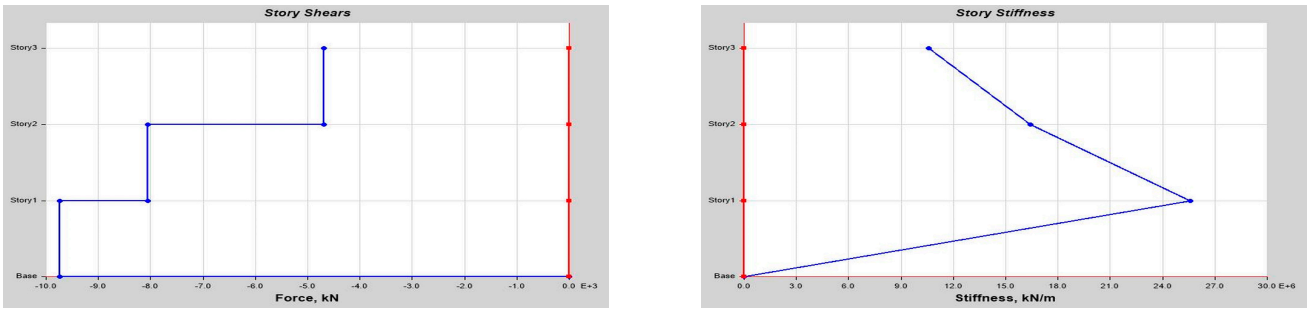


(**a**) (**b**)

**Figure A5.** (**a**) Story shears; (**b**) max story stiffness.

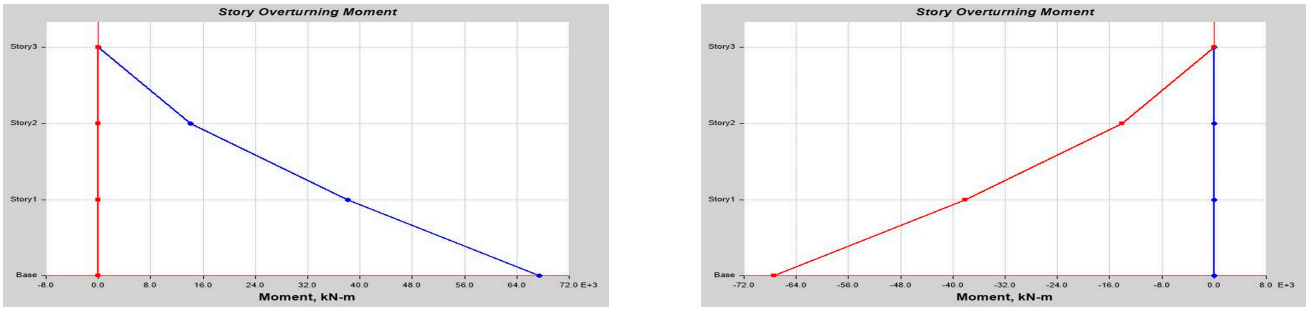


(**a**) (**b**)

**Figure A6.** (**a**) Story overturning moment (X-axis); (**b**) story overturning moment (Y-axis).

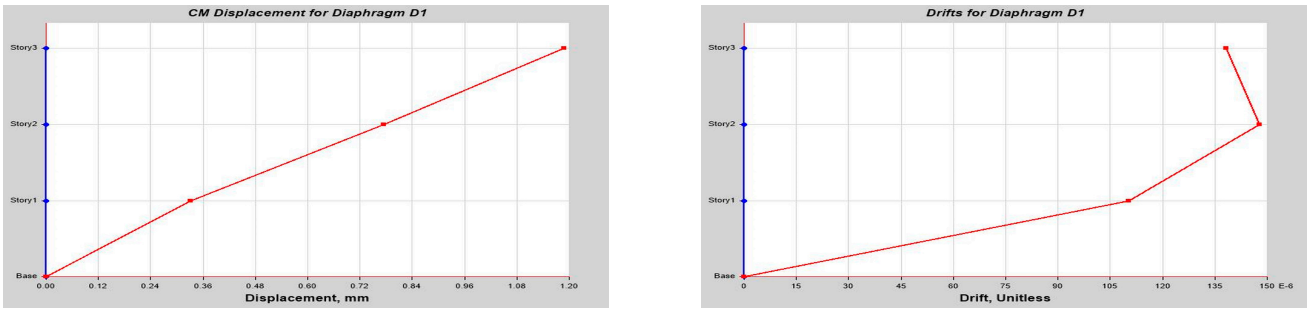


(**a**) (**b**)

**Figure A7.** (**a**) CM displacement for D1 (Y-axis); (**b**) drift for diaphragm D1 (Y-axis).

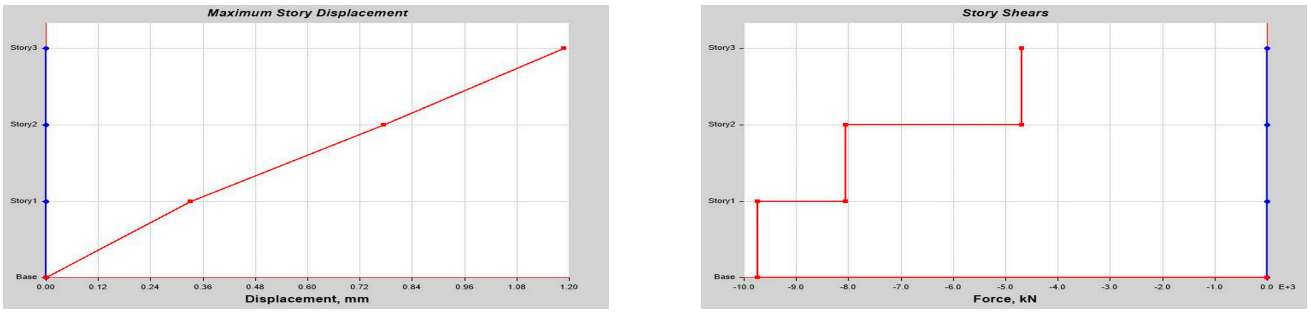


(**a**) (**b**)

**Figure A8.** (**a**) Max story displacement (Y-axis); (**b**) story shears (Y-axis).

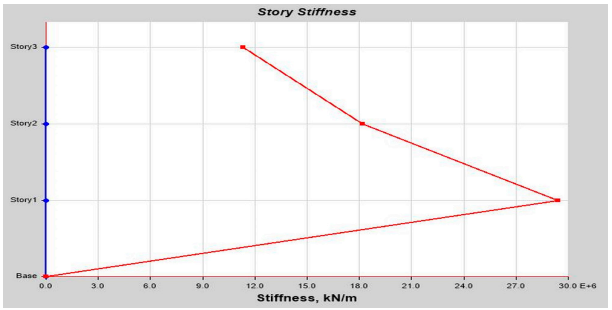


(**a**)

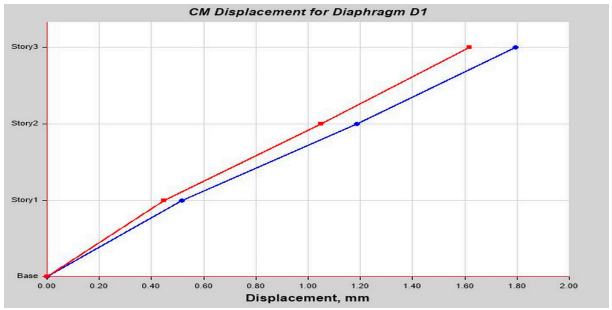


(**b**)

**Figure A9.** (**a**) Story stiffness (Y-axis); (**b**) CM displacement for D1 (X-Y axis).

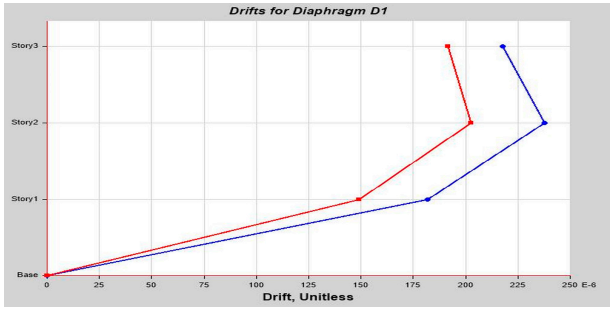


(**a**)

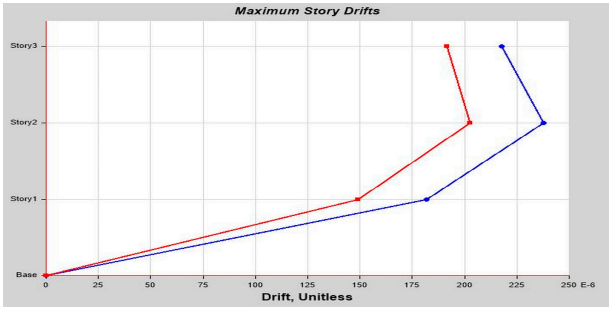


(**b**)

**Figure A10.** (**a**) Drift for diaphragm D1 (X-Y axis); (**b**) max story drifts (X-Y axis).

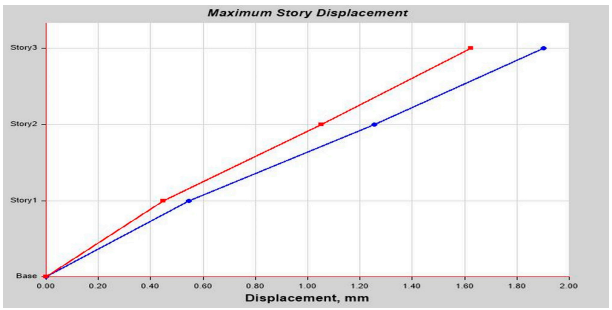


(**a**)


(**b**)

**Figure A11.** (**a**) Max story displacement (X-Y axis); (**b**) story overturning moment (X-Y axis).

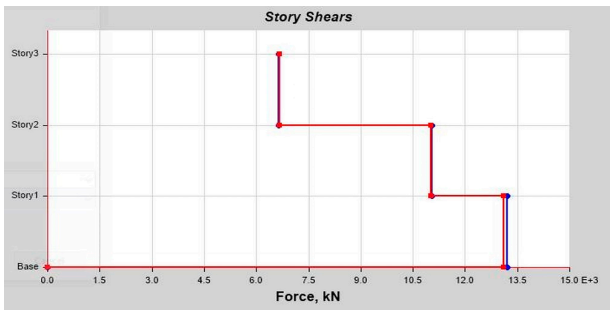


(**a**)

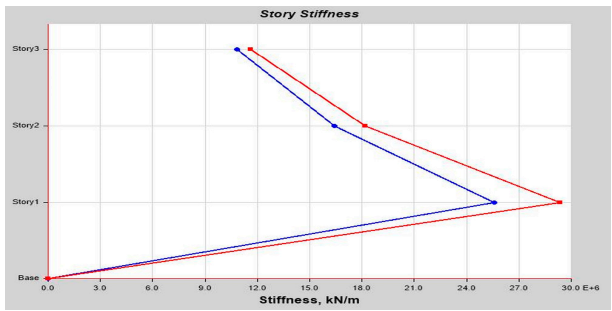


(**b**)

**Figure A12.** (**a**) Story shears (Y-axis); (**b**) story stiffness (X-Y axis).

Six-story sample RC building ETABS output.

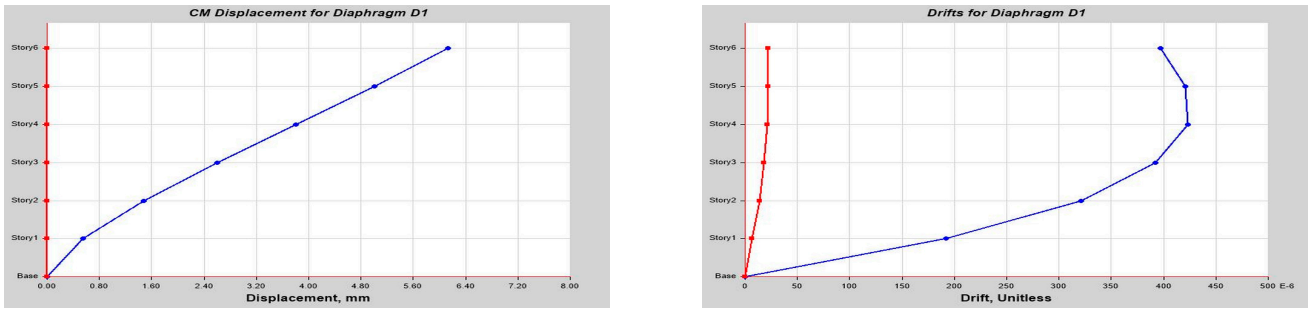


(**a**) (**b**)

**Figure A13.** (**a**) CM displacement for diaphragm D1 (X-axis); (**b**) drifts for diaphragm D1 (X-Y axis).

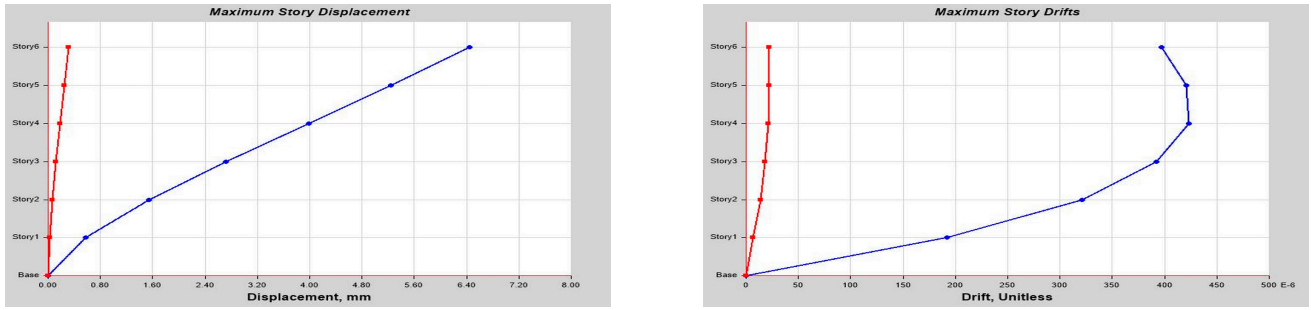


(**a**) (**b**)

**Figure A14.** (**a**) Max story displacement (X-Y axis); (**b**) max story drifts (X-Y axis).

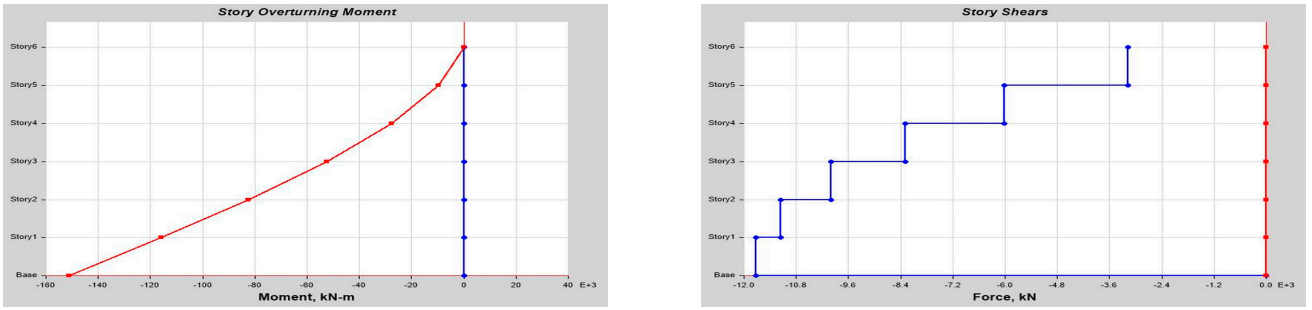


(**a**) (**b**)

**Figure A15.** (**a**) Story overturning moment (Y axis); (**b**) story shears (X-axis).

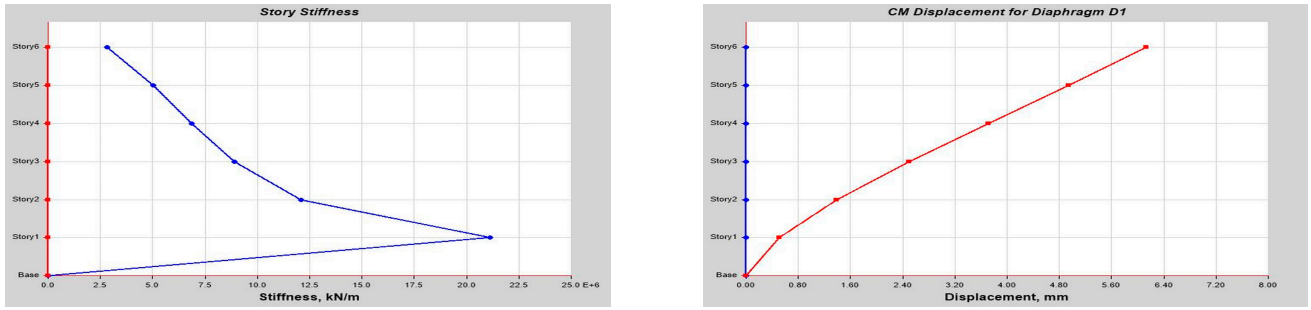


(**a**) (**b**)

**Figure A16.** (**a**) Story stiffness (X-axis); (**b**) CM displacement for diaphragm D1 (X-axis).

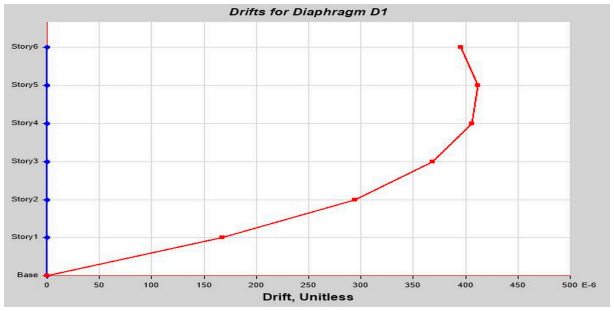


(**a**)

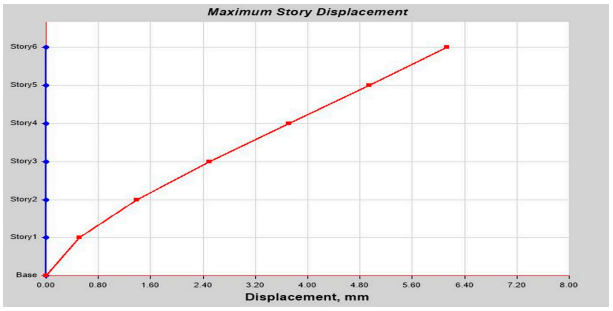


(**b**)

**Figure A17.** (**a**) Drifts for diaphragm D1 (Y-axis); (**b**) max story displacement (Y-axis).

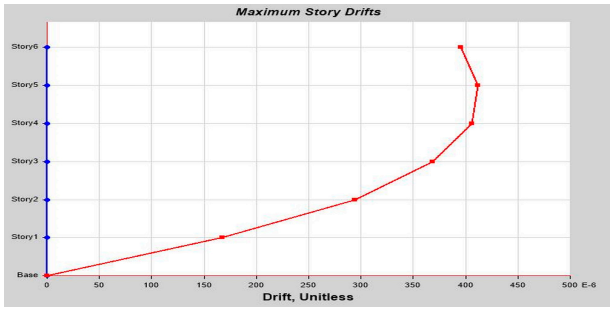


(**a**)

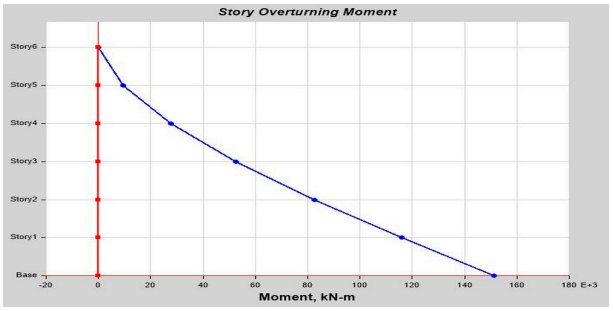


(**b**)

**Figure A18.** (**a**) Max story drifts (Y-axis); (**b**) story overturning moment (X-axis).

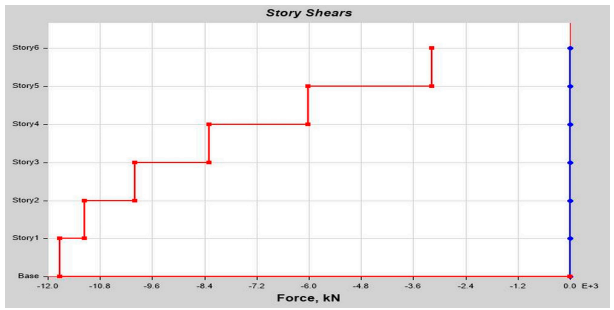


(**a**)

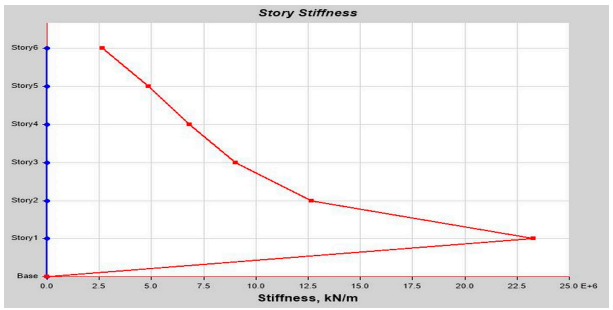


(**b**)

**Figure A19.** (**a**) Story shears (Y-axis); (**b**) story stiffness (Y-axis).

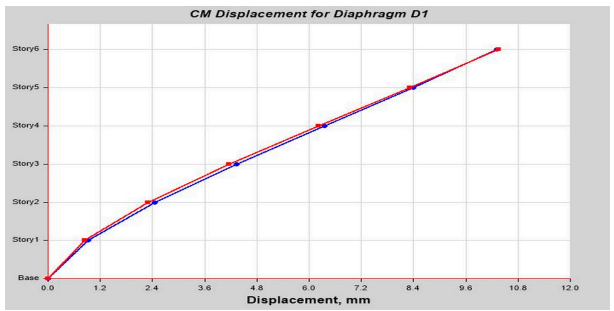


(**a**)

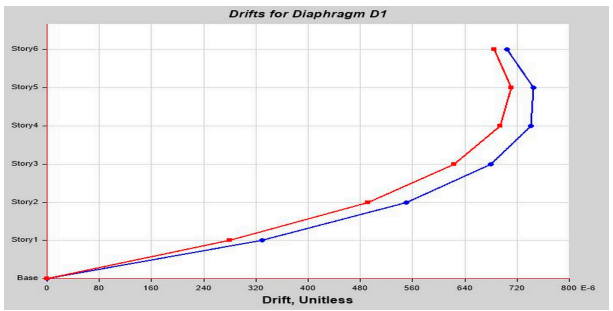


(**b**)

**Figure A20.** (**a**) CM displacement for diaphragm D1 (X-Y axis); (**b**) drifts for diaphragm D1 (X-Y axis).

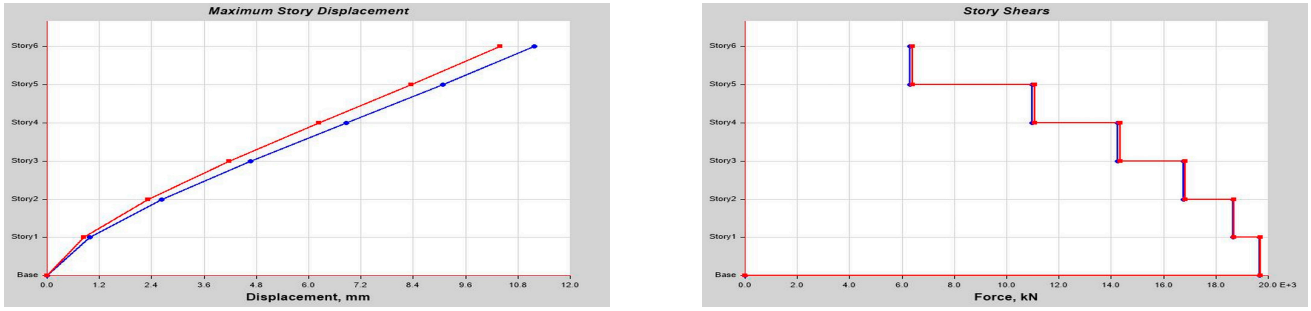


(**a**) (**b**)

**Figure A21.** (**a**) Max story displacement (X-Y axis); (**b**) story shears (X-Y axis).

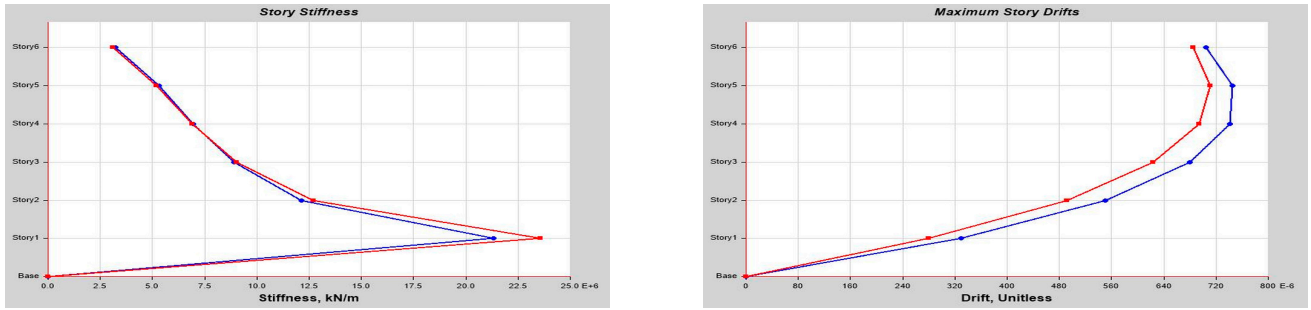


(**a**) (**b**)

**Figure A22.** (**a**) Story stiffness (X-Y axis); (**b**) max story drifts (X-Y axis).

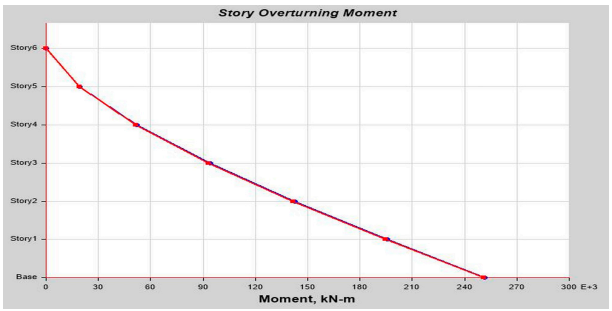


**Figure A23.** Story overturning moment (Y-axis).

Twelve-story sample RC building ETABS output.

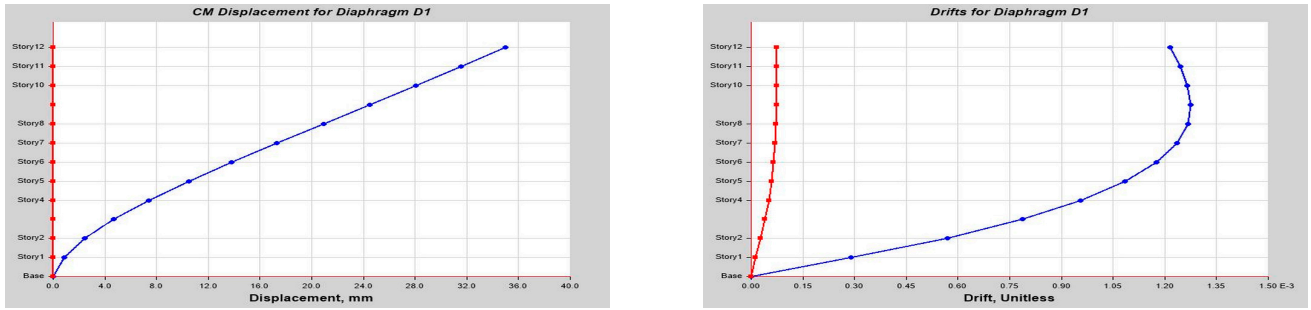


(**a**) (**b**)

**Figure A24.** (**a**) CM displacement for diaphragm D1 (X-axis); (**b**) drifts for diaphragm D1 (X-Y axis).

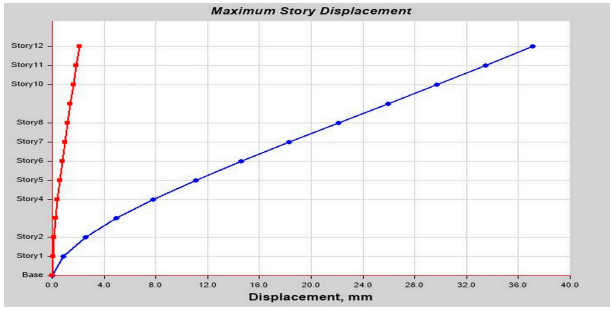


(**a**)

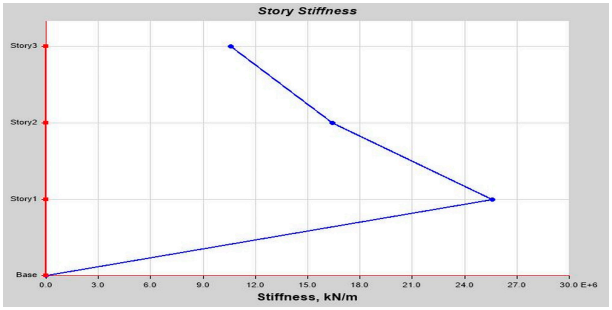


(**b**)

**Figure A25.** (**a**) Max story displacement (X-Y axis); (**b**) max story drifts (X-Y axis).

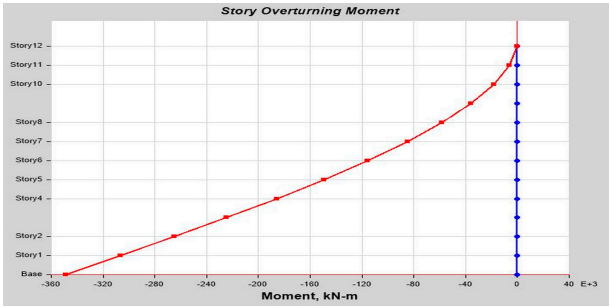


(**a**)

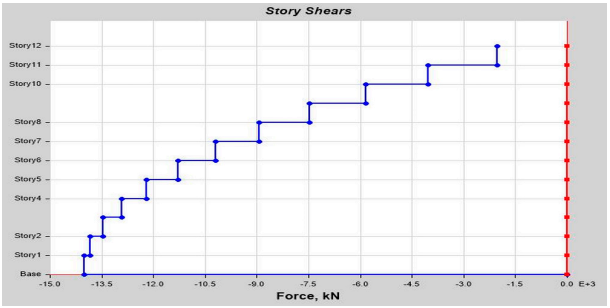


(**b**)

**Figure A26.** (**a**) Story overturning moment (Y-axis); (**b**) story shears (X-axis).

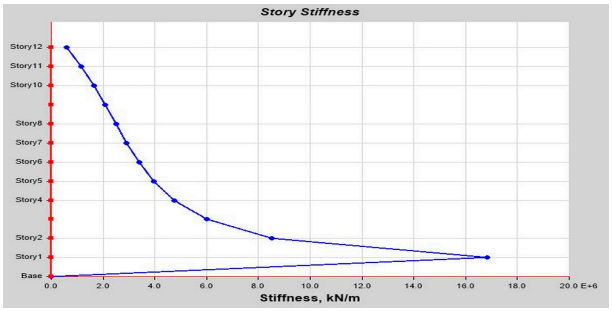


(**a**)

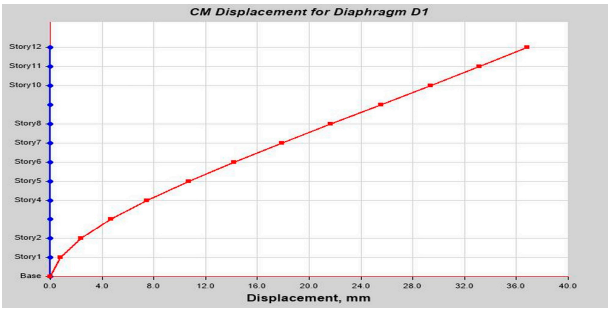


(**b**)

**Figure A27.** (**a**) Story stiffness (X-axis); (**b**) CM displacement for diaphragm D1 (Y-axis).

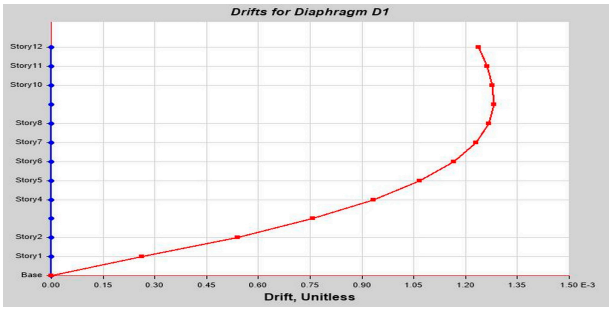


(**a**)

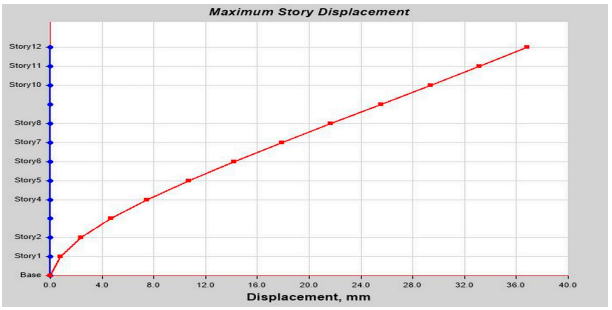


(**b**)

**Figure A28.** (**a**) Drifts for diaphragm D1 (Y-axis); (**b**) max story displacement (Y-axis).

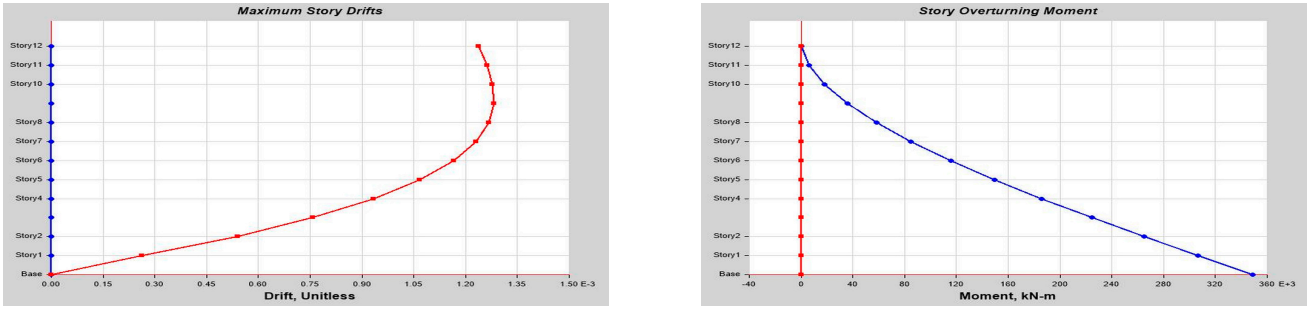


(**a**) (**b**)

**Figure A29.** (**a**) Max story drifts (Y-axis); (**b**) story overturning moment (X-axis).

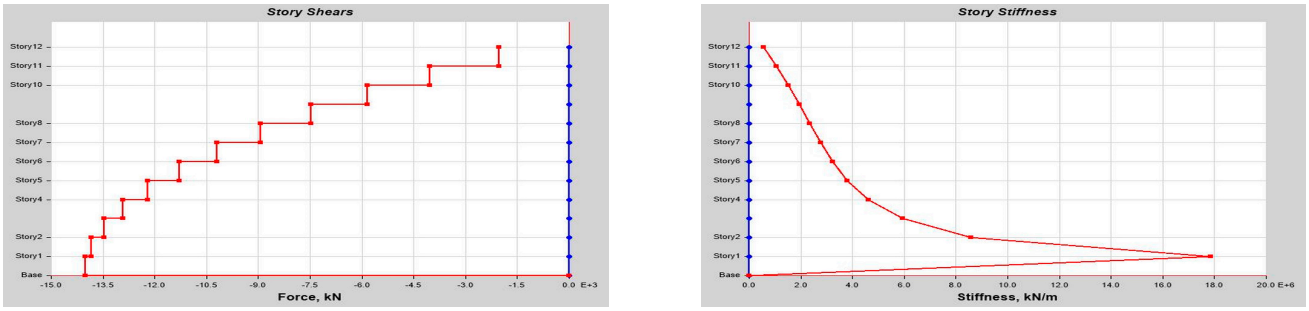


(**a**) (**b**)

**Figure A30.** (**a**) Story shears (Y-axis); (**b**) story stiffness (Y-axis).

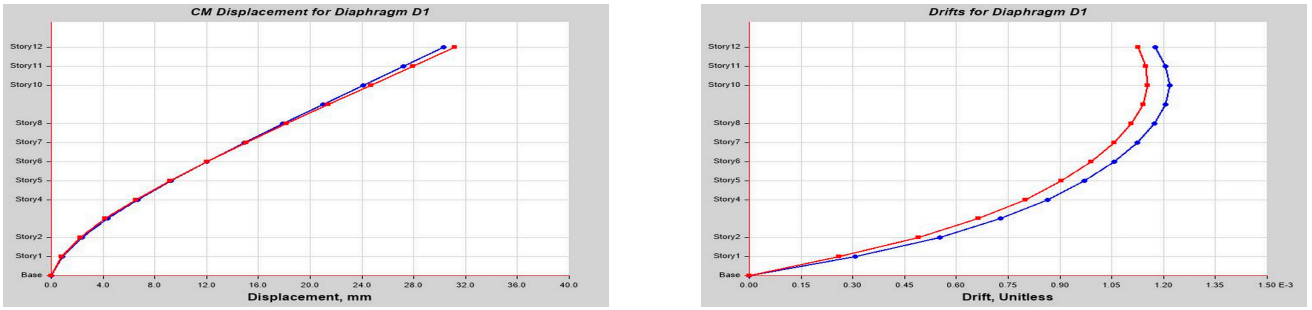


(**a**) (**b**)

**Figure A31.** (**a**) CM displacement for diaphragm D1 (X-Y axis); (**b**) story stiffness (X-Y axis).

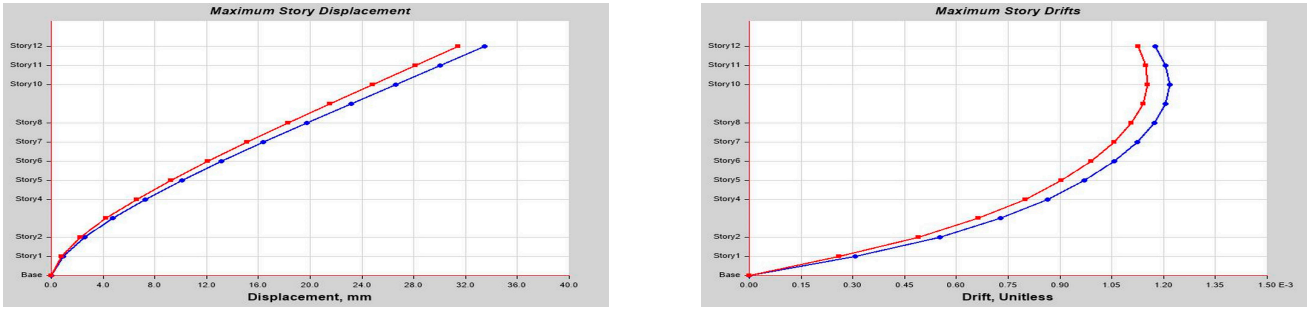


(**a**) (**b**)

**Figure A32.** (**a**) Max story displacement (X-Y axis); (**b**) max story drifts (X-Y axis).

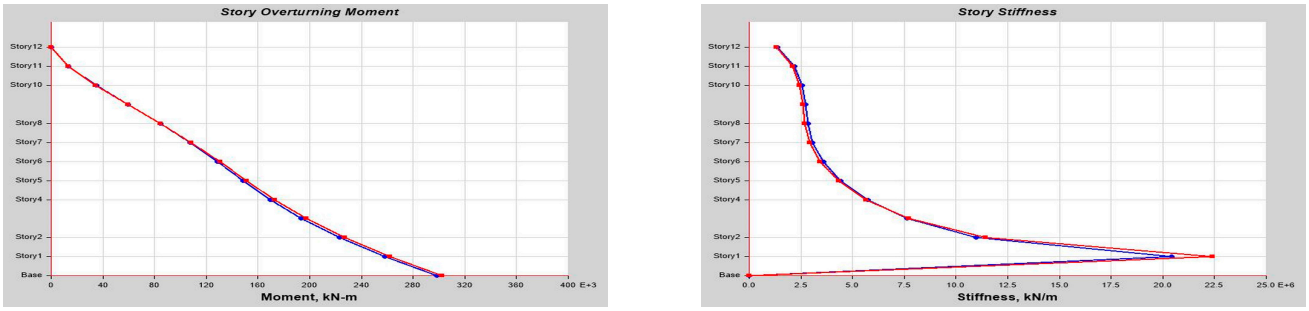


(**a**) (**b**)

**Figure A33.** (**a**) Story overturning moment (X-Y axis); (**b**) story stiffness (X-Y axis).

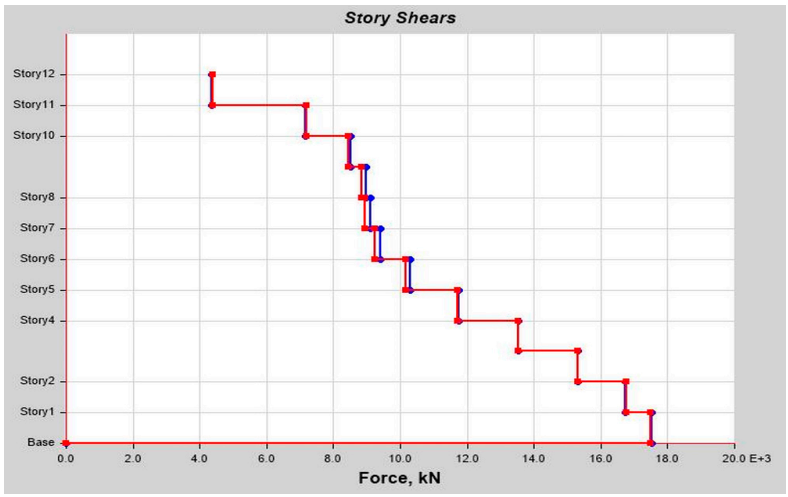


**Figure A34.** Story shears (X-Y axis).

Eighteen-story sample RC building ETABS output.

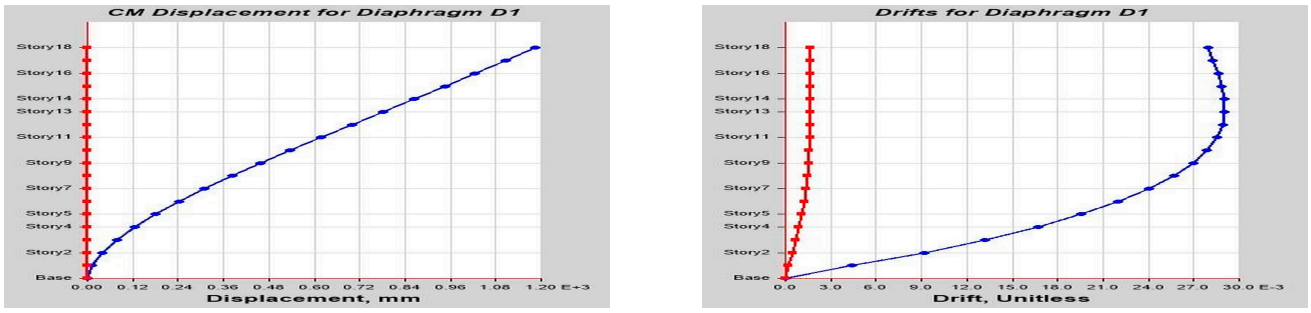


(**a**) (**b**)

**Figure A35.** (**a**) CM displacement for diaphragm D1 (X-axis); (**b**) drifts for diaphragm D1 (X-Y axis).

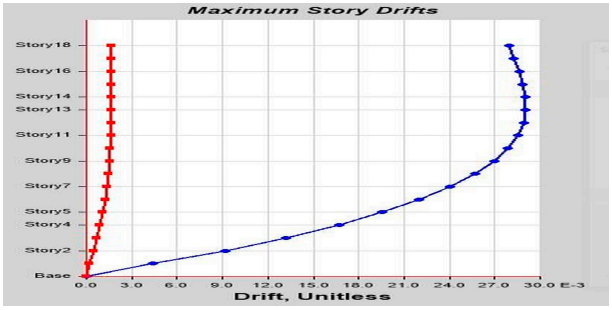


(**a**)

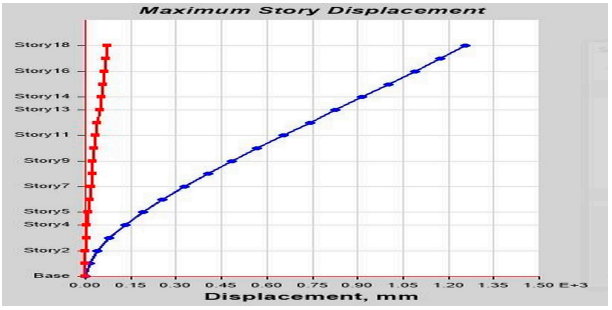


(**b**)

**Figure A36.** (**a**) Max story drifts (X-axis); (**b**) max story displacement (X-Y axis).


(**a**)


(**b**)

**Figure A37.** (**a**) Story overturning moment (Y-axis); (**b**) story shears (X-axis).

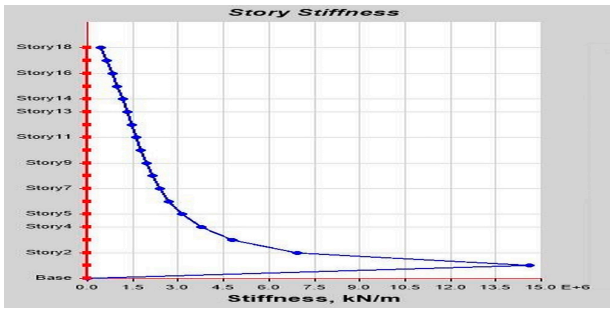


(**a**)

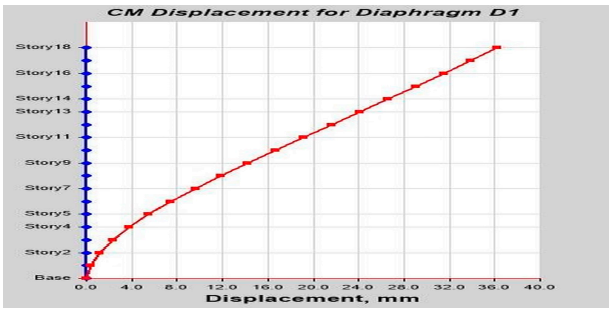


(**b**)

**Figure A38.** (**a**) Story stiffness (X-axis); (**b**) CM displacement for diaphragm D1 (Y-axis).

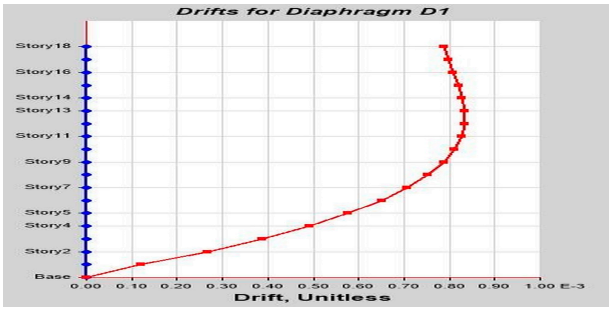


(**a**)

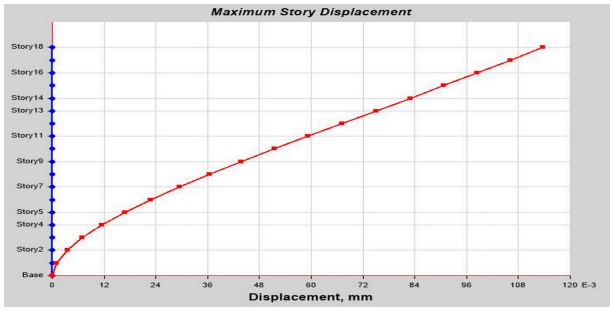


(**b**)

**Figure A39.** (**a**) Drifts for diaphragm D1 (Y-axis); (**b**) max story displacement (Y-axis).

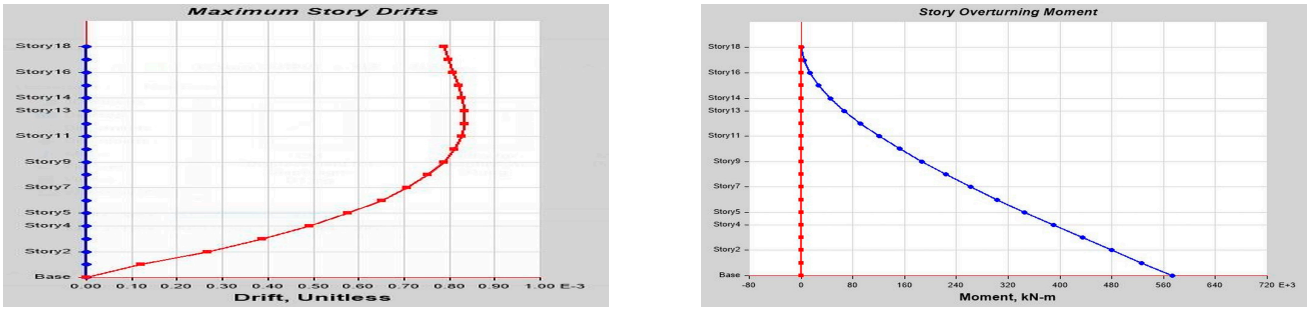


(**a**) (**b**)

**Figure A40.** (**a**) Max story drifts (Y-axis); (**b**) story overturning moment (X-axis).

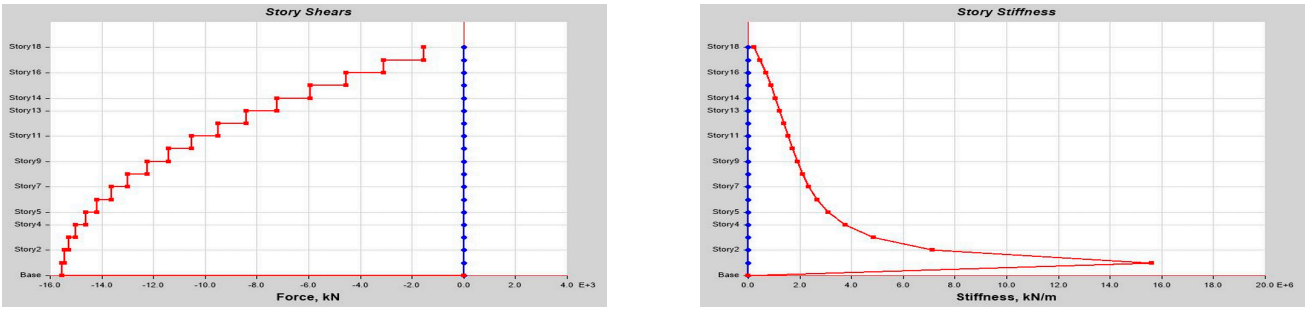


(**a**) (**b**)

**Figure A41.** (**a**) Story shears (Y-axis); (**b**) story stiffness (X-axis).

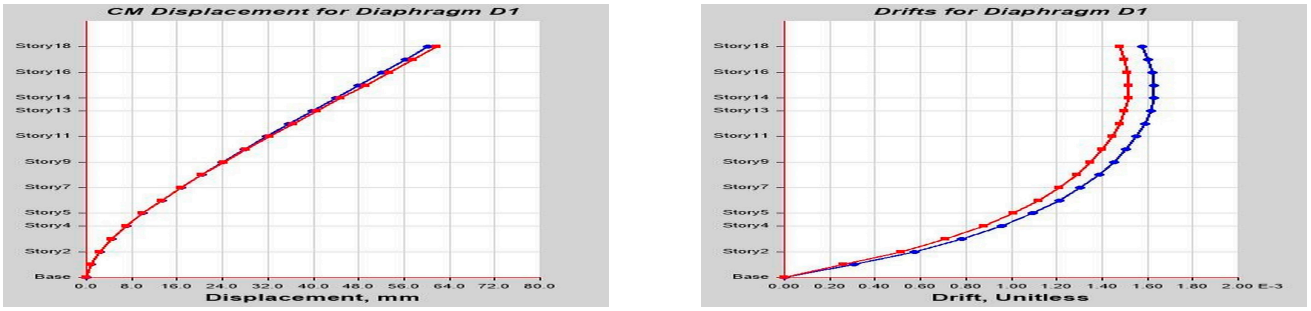


(**a**) (**b**)

**Figure A42.** (**a**) CM displacement for diaphragm D1 (Y-axis); (**b**) drifts for diaphragm D1 (X-Y axis).

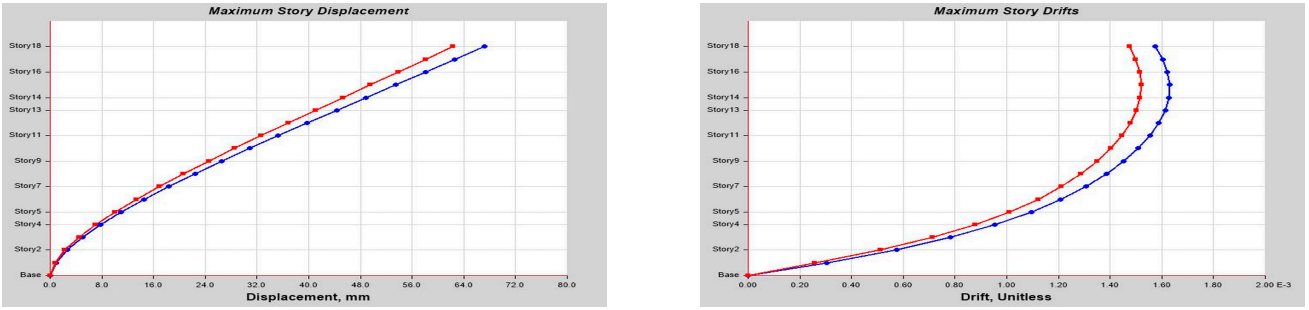


(**a**) (**b**)

**Figure A43.** (**a**) Max story displacement (X-Y axis); (**b**) max story drifts (X-Y axis).

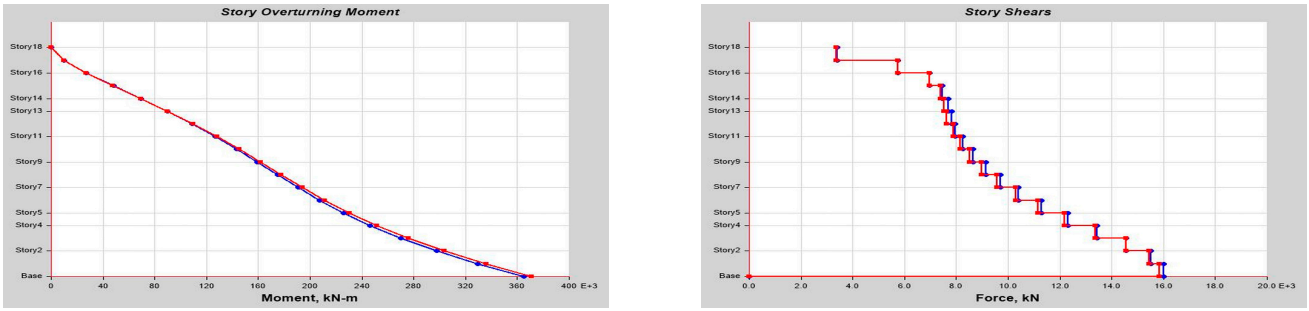


(**a**) (**b**)

**Figure A44.** (**a**) Story overturning moment (X-Y axis); (**b**) story shears (X-Y axis).

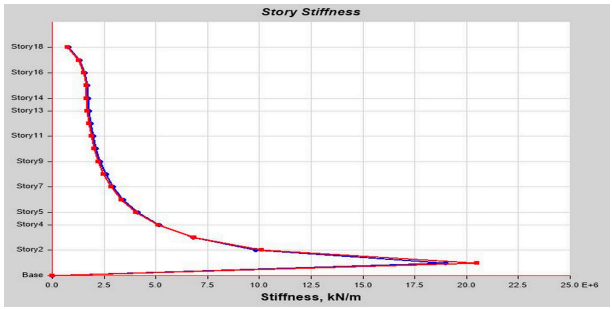


**Figure A45.** Story stiffness (X-Y axis).

## References

1. Sessa, S.; Marmo, F.; Vaiana, N.; Rosati, L. A Computational Strategy for Eurocode 8-Compliant Analyses of Reinforced Concrete Structures by Seismic Envelopes. *J. Earthq. Eng.* **2021**, *25*, 1078–1111. [CrossRef]
2. Najam, F.A.; Warnitchai, P. A modified response spectrum analysis procedure to determine nonlinear seismic demands of high-rise buildings with shear walls. *Struct. Des. Tall Spec. Build.* **2018**, *27*, e1409. [CrossRef]
3. Ghayoumian, G.; Emami, A.R. A multi-direction pushover procedure for seismic response assessment of low-to-medium-rise modern reinforced concrete buildings with special dual system having torsional irregularity. *Structures* **2020**, *28*, 1077–1107. [CrossRef]
4. Oh, S.; Kurama, Y.C.; Mohle, J.; Polster, L.; Manning, M.; Weldon, B. A novel reinforced-concrete buckling-restrained brace for precast concrete lateral-load-resisting frames. *PCI J.* **2023**, *68*, 95–116. [CrossRef]
5. Minas, S.; Galasso, C. Accounting for spectral shape in simplified fragility analysis of case-study reinforced concrete frames. *Soil Dyn. Earthq. Eng.* **2019**, *119*, 91–103. [CrossRef]
6. Aliakbari, F.; Garivani, S.; Aghakouchak, A.A. An energy based method for seismic design of frame structures equipped with metallic yielding dampers considering uniform inter-story drift concept. *Eng. Struct.* **2020**, *205*, 110114. [CrossRef]
7. Ricci, P.; Di Domenico, M.; Verderame, G.M. Behaviour factor and seismic safety of reinforced concrete structures designed according to Eurocodes. *Structures* **2023**, *55*, 677–689. [CrossRef]
8. Dogan, G.; Ecemis, A.S.; Korkmaz, S.Z.; Arslan, M.H.; Korkmaz, H.H. *Buildings Damages after Elazığ, Turkey Earthquake on January 24, 2020*; Springer: Amsterdam, The Netherlands, 2021; Volume 109. [CrossRef]
9. Güneş, N.; Ulucan, Z.Ç. Collapse probability of code-based design of a seismically isolated reinforced concrete building. *Structures* **2021**, *33*, 2402–2412. [CrossRef]
10. Romano, F.; Faggella, M.; Gigliotti, R.; Zucconi, M.; Ferracuti, B. Comparative seismic loss analysis of an existing non-ductile RC building based on element fragility functions proposals. *Eng. Struct.* **2018**, *177*, 707–723. [CrossRef]
11. Lubkowski, Z.; Villani, M.; Coates, K.; Jirouskova, N.; Willis, M. Seismic Design Considerations for East Africa. In Proceedings of the 2nd European Conference of Earthquake Engineering and Seismology, Istanbul, Turkey, 24–29 August 2014; p. 12. Available online: https://www.researchgate.net/publication/279527737_SEISMIC_DESIGN_CONSIDERATIONS_FOR_EAST_AFRICA (accessed on 12 March 2024).
12. Herbert, S. *Assessing Seismic Risk in Ethiopia*; Helpdesk Research Report; GSDRC: Birmingham, UK, 2013; pp. 1–12. Available online: https://assets.publishing.service.gov.uk/media/57a089fd40f0b6497400036e/hdq1087.pdf (accessed on 12 March 2024).
13. Conference, W.; Engineering, E. Seismic Microzonation of Hanoi, Vietnam Using Microtremor Observations. In Proceedings of the 13th World Conference on Earthquake Engineering, Vancouver, BC, Canada, 1–6 August 2004. Available online: https://www.researchgate.net/publication/238605966_SEISMIC_MICROZONATION_OF_HANOI_VIETNAM_USING_MICROTREMOR_OBSERVATIONS (accessed on 12 March 2024).

14. Merajuddin, M.; Azeem, M.A. A Study on Estimation of Stiffness Irregularity in RC buildings. *Int. J. Appl. Eng. Res.* **2020**, *15*, 74–80.
15. Kakpure, G.G.; Mundhada, A.R. Comparative Study of Static and Dynamic Seismic Analysis of Multistoried RCC Buildings by ETAB. *Int. J. Eng. Res. Appl.* **2017**, *7*, 6–10. [CrossRef]
16. Worku, A. Recent Developments in the Definition of Design Earthquake Ground Motions Calling for a Revision of the Current Ethiopian Seismic Code-EBCS 8: 1995. *Zede J.* **2011**, *28*, 1–15.
17. Republic, C. Seismic Hazard of Southern Ethiopia. pp. 2–6. Available online: http://www.geology.cz/projekt681700/popis/Seismic_report_final.pdf (accessed on 12 March 2024).
18. Rift, T.E.; Ale, E. Volcanism and Seismicity + Info. 2021, pp. 3–5. Available online: https://www.nature.com/articles/s41467-021-27166-y (accessed on 12 March 2024).
19. Landge, M.V.; Ingle, R.K. Comparative study of floor response spectra for regular and irregular buildings subjected to earthquake. *Asian J. Civ. Eng.* **2021**, *22*, 49–58. [CrossRef]
20. Syamsi, M.I.; Maulana, T.I.; Widyantama, H.; Ian, M.R.; Lesmana, R.I. Comparative Study of Indonesian Seismic Codes Applied on Vertically Irregular RC Building in High Seismicity Region. *Int. J. Integr. Eng.* **2021**, *13*, 158–167. [CrossRef]
21. Reddy, C.R.; Mothilal, M.; Reddy, C.R. Comparative Study on G + 15 RCC Building with Plan Irregularity Using Response Spectrum Comparative Study on G + 15 RCC Building with Plan Irregularity Using Response Spectrum Analysis and Time History Analysis. 2023. Available online: https://easychair.org/publications/preprint/JbT6 (accessed on 12 March 2024).
22. Ahmad, A.; Riaz, M.; Zafar, T.; Zulfiqar, K.K.; Khawaja, S.A. Comparative Study on Seismic Analysis and Design of High-Rise Buildings Using Static and Dynamic Analysis by Etabs. In Proceedings of the 11th International Civil Engineering Conference, Karachi, Pakistan, 13–14 March 2020; Volume 1, pp. 107–114.
23. Yin, C.; Xie, L.; Li, A.; Zeng, D.; Yang, C.; Wang, X. Comparison of the seismic-resilient design of seismically isolated reinforced concrete frame structures using two codes. *Struct. Des. Tall Spec. Build.* **2021**, *30*, e1886. [CrossRef]
24. Bansal, H. Seismic Analysis and Design of Vertically Irregular RC Building Frames. *Int. J. Sci. Res.* **2014**, *3*, 207–215. Available online: https://www.ijsr.net/archive/v3i8/MDIwMTUyMjE=.pdf (accessed on 12 March 2024).
25. Merino, R.J.; Perrone, D.; Filiatrault, A. Consistent floor response spectra for performance-based seismic design of nonstructural elements. *Earthq. Eng. Struct. Dyn.* **2020**, *49*, 261–284. [CrossRef]
26. Peng, C.; Guner, S. Direct displacement-based seismic assessment of concrete frames. *Comput. Concr.* **2018**, *21*, 355–365. [CrossRef]
27. Ahamad, S.A.; Pratap, K.V. Dynamic analysis of G+20 multi storied building by using shear walls in various locations for different seismic zones by using Etabs. *Mater. Today Proc.* **2020**, *43*, 1043–1048. [CrossRef]
28. Hassan, A.; Pal, S. Effect of soil condition on seismic response of isolated base buildings. *Int. J. Adv. Struct. Eng.* **2018**, *10*, 249–261. [CrossRef]
29. Gkimprixis, A.; Tubaldi, E.; Douglas, J. *Evaluating Alternative Approaches for the Seismic Design of Structures*; Springer: Amsterdam, The Netherlands, 2020; Volume 18. [CrossRef]
30. Sullivan, T.J. Highlighting differences between force-based and displacement-based design solutions for reinforced concrete frame structures. *Struct. Eng. Int. J. Int. Assoc. Bridg. Struct. Eng.* **2013**, *23*, 122–131. [CrossRef]
31. Wang, Z.; Pan, W.; Zhang, Z. High-rise modular buildings with innovative precast concrete shear walls as a lateral force resisting system. *Structures* **2020**, *26*, 39–53. [CrossRef]
32. De Domenico, D.; Falsone, G.; Ricciardi, G. Improved response-spectrum analysis of base-isolated buildings: A substructure-based response spectrum method. *Eng. Struct.* **2018**, *162*, 198–212. [CrossRef]
33. Priestley, M.J.N. Does capacity design do the job? *Bull. N. Z. Soc. Earthq. Eng.* **2003**, *36*, 276–292. [CrossRef]
34. Crowley, H.; Despotaki, V.; Silva, V.; Dabbeek, J.; Romão, X.; Pereira, N.; Castro, J.M.; Daniell, J.; Veliu, E.; Bilgin, H.; et al. Model of seismic design lateral force levels for the existing reinforced concrete European building stock. *Bull. Earthq. Eng.* **2021**, *19*, 2839–2865. [CrossRef]
35. Khy, K.; Chintanapakdee, C.; Warnitchai, P.; Wijeyewickrema, A.C. Modified response spectrum analysis to compute shear force in tall RC shear wall buildings. *Eng. Struct.* **2019**, *180*, 295–309. [CrossRef]
36. Esfandiari, M.J.; Urgessa, G.S. Progressive collapse design of reinforced concrete frames using structural optimization and machine learning. *Structures* **2020**, *28*, 1252–1264. [CrossRef]
37. Afzal, M.; Liu, Y.; Cheng, J.C.P.; Gan, V.J.L. Reinforced concrete structural design optimization: A critical review. *J. Clean. Prod.* **2020**, *260*, 120623. [CrossRef]
38. Zhao, W.; Qian, J. Resistance mechanism and reliability analysis of reinforced concrete columns subjected to lateral impact. *Int. J. Impact Eng.* **2020**, *136*, 103413. [CrossRef]
39. Kangle, S.R. Response Spectrum Analysis for Regular Multistory Structure in Seismic Zone III. *Int. J. Eng. Res.* **2020**, *V9*, 478–483. [CrossRef]
40. Vishal, N.; Ramesh Kannan, M.; Keerthika, L. Seismic Analysis of Multi-Storey Irregular Building with Different Structural Systems. *Int. J. Recent Technol. Eng.* **2020**, *8*, 3146–3155. [CrossRef]
41. Rodrigues, H.; Furtado, A.; Vila-Pouca, N.; Varum, H.; Barbosa, A.R. Seismic Assessment of a School Building in Nepal and Analysis of Retrofitting Solutions. *Int. J. Civ. Eng.* **2018**, *16*, 1573–1589. [CrossRef]
42. Sharma, P.; Gupta, T. Comparative Investigation on Mode Shapes and Natural Frequency of Low-Rise RC Frame Building. In *Advances in Construction Materials and Sustainable Environment*; Springer: Amsterdam, The Netherlands, 2021; pp. 6–11.

43. Hu, S.; Wang, W.; Qu, B. Seismic economic losses in mid-rise steel buildings with conventional and emerging lateral force resisting systems. *Eng. Struct.* **2020**, *204*, 110021. [CrossRef]
44. Xu, C.; Deng, J.; Peng, S.; Li, C. Seismic fragility analysis of steel reinforced concrete frame structures based on different engineering demand parameters. *J. Build. Eng.* **2018**, *20*, 736–749. [CrossRef]
45. Aggarwal, Y.; Saha, S.K. Seismic performance assessment of reinforced concrete hilly buildings with open story. *Structures* **2021**, *34*, 224–238. [CrossRef]
46. Rahman, M.M.; Jadhav, S.M.; Shahrooz, B.M. Seismic performance of reinforce concrete buildings designed according to codes in Bangladesh, India and U.S. *Eng. Struct.* **2018**, *160*, 111–120. [CrossRef]
47. Shah, A.; Ahmad, S. Analysis of Seismic Behavior of Buildings with and without Shear Walls in Various Seismic Zones and Soil Types. In *Advances in Construction Materials and Sustainable Environment*; Springer: Amsterdam, The Netherlands, 2021; pp. 6–11.
48. Iervolino, I.; Spillatura, A.; Bazzurro, P. Seismic Reliability of Code-Conforming Italian Buildings. *J. Earthq. Eng.* **2018**, *22*, 5–27. [CrossRef]
49. Thomas, R.K.; Philip, S.E.; Vasugi, V. Comparative Study on Seismic Behaviour of G+41 Storey Frame with X, K and V Bracings. *Lect. Notes Civ. Eng.* **2022**, *175*, 127–133. [CrossRef]
50. Samanta, A.; Swain, A. Seismic Response and Vulnerability Assessment of Representative Low, Medium and High-rise Buildings in Patna, India. *Structures* **2019**, *19*, 110–127. [CrossRef]
51. Martin, A.; Deierlein, G.G. Structural topology optimization of tall buildings for dynamic seismic excitation using modal decomposition. *Eng. Struct.* **2020**, *216*, 110717. [CrossRef]
52. Lim, H.K.; Kang, J.W.; Pak, H.; Chi, H.S.; Lee, Y.G.; Kim, J. Seismic response of a three-dimensional asymmetric multi-storey reinforced concrete structure. *Appl. Sci.* **2018**, *8*, 479. [CrossRef]
53. Masi, A.; Santarsiero, G.; Manfredi, V.; Biondi, S.; Spacone, E.; Del Gaudio, C.; Ricci, P.; Manfredi, G.; Verderame, G.M. Seismic response of RC buildings during the Mw 6.0 August 24, 2016 Central Italy earthquake: The Amatrice case study. *Bull. Earthq. Eng.* **2019**, *17*, 5631–5654. [CrossRef]
54. Arabzadeh, H.; Galal, K. Seismic-Response Analysis of RC C-Shaped Core Walls Subjected to Combined Flexure, Shear, and Torsion. *J. Struct. Eng.* **2018**, *144*, 4. [CrossRef]
55. Martins, A.M.B.; Simões, L.M.C.; Negrão, J.H.J.O.; Lopes, A.V. Sensitivity analysis and optimum design of reinforced concrete frames according to Eurocode 2. *Eng. Optim.* **2020**, *52*, 2011–2032. [CrossRef]
56. Esteghamati, M.Z.; Banazadeh, M.; Huang, Q. The effect of design drift limit on the seismic performance of RC dual high-rise buildings. *Struct. Des. Tall Spec. Build.* **2018**, *27*, e1464. [CrossRef]
57. Isik, E.; Harirchian, E.; Bilgin, H.; Jadhav, K. The effect of material strength and discontinuity in RC structures according to different site-specific design spectra. *Res. Eng. Struct. Mater.* **2021**, *7*, 413–430. [CrossRef]
58. Saharia, R.; Bhuyan, D.; Chowdhury, S.; Bharadwaj, K. Comparative Study on Static and Dynamic Analysis of RC Buildings of Different Heights in Different Seismic Zones. *Lect. Notes Civ. Eng.* **2022**, *175*, 161–174. [CrossRef]
59. Mahmoud, S.; Abdallah, W. Response Analysis of Multi-Storey RC Buildings under Equivalent Static and Dynamic Loads According to Egyptian Code. *Int. J. Civ. Struct. Eng. Res.* **2014**, *2*, 79–88.
60. Islam, Z.; Tarin, A.S. Earthquake response analysis of a multistoried RC building under equivalent static and dynamic loading as per Bangladesh national building code 2006. *Malays. J. Civ. Eng.* **2016**, *28*, 108–123.
61. Latifi, R.; Hadzima-Nyarko, M. A comparison of structural analyses procedures for earthquake-resistant design of buildings. *Earthq. Struct.* **2021**, *20*, 531–542. [CrossRef]
62. SAP. *Static and Dynamic Finite Element Analysis of Structures, Version 19.0*; Computers and Structures; ETABS: Berkeley, CA, USA, 2019. Available online: https://www.csiamerica.com/ (accessed on 12 March 2024).
63. *ES EN 1998-1:2015*; Eurocode 8: Design of Structures for Earthquake Resistance—Part 1: General Rules, Seismic Actions and Rules for Buildings. European Committee for Standardization: Brussels, Belgium, 2015. Available online: https://www.phd.eng.br/wp-content/uploads/2015/02/en.1998.1.2004.pdf (accessed on 5 April 2023).